Simulating Floquet dynamics with variational quantum eigensolvers

Masterarbeit
zur Erlangung des akademischen Grades
Master of Science
im Studiengang Physik
der Naturwissenschaftlichen Fakultät NT
- Physik -
der Universität des Saarlandes

von

Niklas Jung

Saarbrücken, Oktober 2023

Erklärung

Hiermit versichere ich, dass ich die vorliegende Arbeit selbstständig verfasst und keine anderen als die angegebenen Quellen und Hilfsmittel benutzt habe.

Niklas Jung
Saarbrücken,

Acknowledgements

I would like to thank Prof. Wilhelm-Mauch for the possibility to write this thesis with him as supervisor.

Furthermore I would like to thank Benedikt Fauseweh and Peter Schuhmacher, who supervised me and helped me a lot with both numerical and analytical problems and supported me in my writing.

I would also like to thank the Institute for Software Technology at DLR for making it possible to work on this thesis, and especially the QCA group for a nice work atmosphere and support.

I would like to thank my friends, especially those who supported me with my thesis and took the time to talk with me about problems and review my thesis.

I thank my family for their continued support throughout my academic career.

Furthermore, I thank Prof. Orth, who has agreed to take on the role as second examiner.

Contents

1 Introduction

In recent years there has been an immense research activity aimed at understanding the detailed dynamics of quantum systems exposed to strong time-dependent external fields. Examples include light-induced surface states [1], topological phases of matter [2, 3] and photo-induced superconductivity [4]. The quantum mechanics of explicitly time-dependent Hamiltonians generates a variety of novel phenomena not accessible within ordinary stationary quantum mechanics [5].

If the external field is periodic in time, it is convenient to use the Floquet formalism to study the arising dynamics. The solutions for such systems, as the solution of the time-dependent Schrödinger equation, reduce to eigenvalue equations for the *Floquet quasi-energies*, from which properties of the system can then be derived. Although this formalism is a well-performing tool to treat time-periodic Hamiltonians, these eigenvalue equations are not analytically solvable in most cases. This means that to compute the quasi-energies, one generally has to apply numerical methods. There exist various techniques to tackle this on a classical computer, but most are either not universally applicable or their runtime scales exponentially with system size [6].

In quantum mechanics, there are a lot of problems that cannot be solved efficiently on a classical computer. A prominent example is the correlation of measurement results of two entangled photons [7]. For this reason it has been proposed to use quantum systems as computers to overcome those limitations of classical computers. The emerging field of *quantum information* deals with the research and the possible realization of such a device, called a *quantum computer* [8]. There are multiple paradigms of quantum computation. The most famous one is the gate-based model. Gate-based quantum computers use *quantum bits*, or *qubits*, which are the analogon to the classical bit on a classical computer. A qubit is a quantum mechanical two-level system, whose base states represent the respective 0 and 1 states of a classical bit. Instead of just a two-level system, there is also the possibility to have a system with more than two basis states, which is then called a *qudit*. Operations on a quantum computer are represented by *gates*, which are unitary operators acting on one or multiple qubits or qudits. A quantum algorithm then consists of a sequence of gates, the *circuit*, which implements the algorithm and measurements to obtain the results. If a quantum circuit depends on externally set parameters, it is called a *parametrized quantum circuit*.

However, currently available quantum devices have several problems. Noise and qubit limitations severely constrain the implementability of many quantum algorithms [9]. Current devices, which we refer to as *noisy intermediate-scale quantum (NISQ)* devices, have been argued to be able to outperform classical computers in certain mathematical tasks, but speed-up for practical applications has yet to be realized. To address this, the strategy of *variational quantum algorithms*, among others, has emerged, which accounts for the constraints imposed by NISQ devices by combining classical and quantum resources [10]. To achieve that, the problem is first encoded into a cost function. Then, a parametrized quantum circuit is used to evaluate this cost function which is

then optimized on a classical computer. The parametrization, i.e. the gates and the variational parameters, of the quantum circuit is called the *ansatz* for the variational quantum algorithm. Constructing the ansatz is an important part of variational quantum computing, since the ansatz determines the precision and the runtime of the algorithm [10].

In this work, we present the Fauseweh-Zhu-2 algorithm as a possibility to treat a quantum system with a time-dependent, periodic Hamiltonian using such a variational quantum algorithm. We especially focus on finding an efficient ansatz construction scheme for a mixed qubit-qudit architecture, which we implement and evaluate for this algorithm.

We approach this by first discussing the theoretical background in section 2. We first explain Floquet theory in general and then discuss a numerical method to treat it, namely the method of Floquet matrix. After that, variational quantum algorithms (VQAs) are presented, where we first explain the principle of variational quantum algorithms and then look into the variational quantum eigensolver (VQE) as a special case of a VQA. We then explain the Fauseweh-Zhu-2 algorithm as an specific VQA for treating Floquet dynamics. We then discuss one way for the diagrammatic construction of an ansatz to use with the VQE using perturbation theory. In section 3 we then discuss a way to improve the algorithm presented in section 2. We show a way to algorithmically implement the diagrammatic ansatz construction scheme and present another, more general scheme. We then combine both these methods to find an ansatz construction scheme for a mixed qubit-qudit architecture. We implement and evaluate the Fauseweh-Zhu-2 algorithm using the constructed ansatz in section 4, and compare it to a general, not problem-specific ansatz. We see that the systematically constructed ansatz performs better than the general ansatz for simple examples.

2 Theoretical Foundations

In this section we first introduce the theoretical foundations of time-dependent interactions and Floquet theory in section 2.1. First, we review its theoretical background in section 2.1.1, and then look at the method of Floquet matrix as a way to treat it numerically in section 2.1.2. We review the concept of variational quantum algorithms in section 2.2, specifically variational quantum eigensolvers, as a way to treat this numerical problem. We present a general outline for a variational quantum algorithm in section 2.2.1 and the principle for variational quantum eigensolvers in section 2.2.2, as well as the significance of the ansatz state in section 2.2.3. We present the Fauseweh-Zhu-2 algorithm as a particular variational quantum algorithm for solving Floquet dynamics using the method of Floquet matrix in section 2.2.4. Following that, we study the problem of finding a suitable ansatz for a variational quantum algorithm. We first explain some theoretical foundations for ansatz construction in section 2.3.1 and then present a problem-specific diagrammatic method to construct an ansatz in section 2.3.2. For the purposes of comparison, we also present a general, not problem-specific ansatz in section 2.3.3.

2.1 Floquet theory

In this section we introduce Floquet theory as a way to solve the time-dependent Schrödinger equation. Let f be a function in t, A be an operator depending on t and $c \in \mathbb{C}$ be a constant. We first consider a differential equation of the form

$$A(t)f(t) = c\frac{\mathrm{d}}{\mathrm{d}t}f(t) \tag{1}$$

where $A(t)$ is periodic in t, so $A(t) = A(t+T)$ with a period T. The Floquet theorem [11] now implies that there exist solutions f_α to eq. (1) that are of the form

$$f_\alpha(t) = \exp\left(\frac{1}{c}\epsilon_\alpha t\right) g_\alpha(t). \tag{2}$$

with a periodic function $g_\alpha(t+T) = g_\alpha(t)$.

2.1.1 Floquet formalism

Using this result, we can characterize solutions to the Schrödinger equation of a system with a time-periodic Hamiltonian [5]. We consider a quantum system with its Hamiltonian being a periodic function of time,

$$H(x,t) = H(x,t+T), \tag{3}$$

where T again denotes the period. The Schrödinger equation for the quantum system may be written as

$$\left(H(x,t) - i\hbar\frac{\partial}{\partial t}\right)\Psi(x,t) = 0 \tag{4}$$

with

$$H(x,t) = H_0(x) + V(x,t), \qquad V(x,t) = V(x,t+T). \tag{5}$$

The unperturbed Hamiltonian $H_0(x)$ is assumed to possess a complete orthonormal set of eigenfunctions $\{\varphi(x)\}$ with corresponding eigenvalues $\{E_n\}$. We can now apply the Floquet theorem. According to eq. (2) there exist solutions to eq. (4) that have the form

$$\Psi_\alpha(x,t) = \exp(-i\epsilon_\alpha t/\hbar)\Phi_\alpha(x,t), \tag{6}$$

where $\Phi_\alpha(x,t)$ is periodic in time, so it obeys

$$\Phi_\alpha(x,t) = \Phi_\alpha(x,t+T). \tag{7}$$

We call Φ_α a **Floquet mode**, where ϵ_α is a real parameter unique up to multiples of $\hbar\Omega$, with $\Omega = 2\pi/T$ denoting the driving frequency, and is called the **Floquet quasienergy**. The functions $\Psi_\alpha(x,t)$ are called **Floquet-state solutions**.
Introducing the Hermitian operator

$$\mathcal{H}(x,t) \equiv H(x,t) - i\hbar\frac{\partial}{\partial t} \tag{8}$$

one finds that

$$\mathcal{H}(x,t)\Phi_\alpha(x,t) = \epsilon_\alpha\Phi_\alpha(x,t). \tag{9}$$

We notice that the Floquet modes

$$\Phi_{\alpha'}(x,t) = \Phi_\alpha(x,t)\exp(ij\Omega t) \equiv \Phi_{\alpha,j}(x,t) \tag{10}$$

with $j \in \mathbb{Z}$ yield the identical solution to that in eq. (6), but with shifted quasienergy

$$\epsilon_{\alpha'} = \epsilon_\alpha + j\hbar\Omega \equiv \epsilon_{\alpha,j}. \tag{11}$$

Hence, the index α corresponds to a class of solutions indexed by $\alpha' = (\alpha, n)$. The eigenvalues $\{\epsilon_\alpha\}$ therefore can be mapped onto a first Brillouin zone obeying $-\hbar\Omega/2 \leq \epsilon < \hbar\Omega/2$.
For the operator $\mathcal{H}$ it is convenient to introduce the composite Hilbert space $\mathcal{R}\otimes\mathcal{T}$ made up of the Hilbert space $\mathcal{R}$ of square integrable functions on configuration space and the space $\mathcal{T}$ of function which are periodic in t with period $T = 2\pi/\Omega$.
The inner product for the spatial part is defined by

$$\langle\phi|\psi\rangle \equiv \int \mathrm{d}x\, \phi^*(x)\psi(x). \tag{12}$$

We therefore get that

$$\langle\varphi_n|\varphi_m\rangle \equiv \int \mathrm{d}x\, \varphi_n^*(x)\varphi_m(x) = \delta_{n,m}. \tag{13}$$

The temporal part is spanned by the orthonormal set of Fourier vectors $\langle t|j\rangle \equiv \exp(-ij\Omega t), n \in \mathbb{Z}$ and their inner product in $\mathcal{T}$ reads

$$\langle k|j\rangle = \frac{1}{T}\int_0^T \mathrm{d}t \exp[-i(j-k)\Omega t] = \delta_{k,j}. \tag{14}$$

This means that the eigenvectors $|\Phi_\alpha\rangle$ of $\mathcal{H}$ obey the orthonormality condition on the composite Hilbert space $\mathcal{R}\otimes\mathcal{T}$,

$$\big\langle\big\langle \Phi_{\alpha'}(t)\big|\Phi_{\beta'}(t)\big\rangle\big\rangle \equiv \frac{1}{T}\int_0^T \mathrm{d}t \int_{-\infty}^{\infty} \mathrm{d}x \Phi_{\alpha'}^*(x,t)\Phi_{\beta'}(x,t) = \delta_{\alpha',\beta'} = \delta_{\alpha,\beta}\delta_{n,m}, \tag{15}$$

and form a complete set in $\mathcal{R}\otimes\mathcal{T}$.

2.1.2 Numerical approach

In most cases, a quantum system with explicitly time-dependent interaction potentials cannot be solved exactly. In general we therefore have to invoke numerical procedures.

Method of Floquet matrix

To solve for the quasienergies, we can expand the Floquet solutions into the Fourier vectors $|j\rangle,\ j \in \mathbb{Z}$, such that $\langle t|j\rangle = \exp(-ij\Omega t)$. The Fourier vectors $\{|j\rangle\}_{j\in\mathbb{Z}}$ form a basis of $\mathcal{T}$

$$\Phi_\alpha(x,t) = \sum_{j=-\infty}^{\infty} c_\alpha^{(j)}(x)\exp(-ij\Omega t). \tag{16}$$

The functions $c_\alpha^{(j)}(x)$ can furthermore be expanded in terms of the unperturbed eigenfunctions of $H_0(x)$, namely $\{\varphi_n(x), n \in \mathbb{N}\}$, which yields

$$\Phi_\alpha(x,t) = \sum_{n=1}^{\infty}\sum_{j=-\infty}^{\infty} c_{\alpha,n}^{(j)}(x)\varphi_n(x)\exp(-ij\Omega t), \tag{17}$$

with $c_{\alpha,n}^{(j)} = \left\langle \varphi_n \middle| c_\alpha^{(j)} \right\rangle$. The Floquet equation in bra-ket notation then reads

$$\sum_{n=1}^{\infty}\sum_{j=-\infty}^{\infty} \mathcal{H} c_{\alpha,n}^{(j)}|j\rangle|\varphi_n\rangle = \sum_{n=1}^{\infty}\sum_{j=-\infty}^{\infty} \epsilon_\alpha c_{\alpha,n}^{(j)}|j\rangle|\varphi_n\rangle, \tag{18}$$

where we used the operator $\mathcal{H}$ as defined in eq. (8). We now multiply this equation with $\langle\varphi_m|\langle k|$ from the left. This yields

$$\sum_{n=1}^{\infty}\sum_{j=-\infty}^{\infty} \langle\varphi_m|\langle k|\mathcal{H}|j\rangle|\varphi_n\rangle c_{\alpha,n}^{(j)} = \epsilon_\alpha c_{\alpha,m}^{(k)}, \tag{19}$$

where we used the scalar product notation from eq. (15).
Using eq. 14, we can now explicitly calculate the scalar product, keeping in mind that $|\phi_j\rangle$ is time-independent. We write

$$\begin{aligned}\langle\varphi_m|\langle k|\mathcal{H}|j\rangle|\varphi_n\rangle &= \langle\varphi_m|\left(\frac{1}{T}\int_0^T \exp(ik\Omega t)\mathcal{H}\exp(-ij\Omega t)\right)|\varphi_n\rangle \\ &= \langle\varphi_m|\frac{1}{T}\int_0^T H(t)\exp[-i(j-k)\Omega t]|\varphi_n\rangle \\ &- \langle\varphi_m|\underbrace{\frac{1}{T}\int_0^T \exp(ik\Omega t)i\hbar\frac{\partial}{\partial t}\exp(-ij\Omega t)}_{=-n\hbar\Omega\delta_{j,k}}|\varphi_n\rangle. \end{aligned} \tag{20}$$

We now define

$$H^{j-k} \equiv \langle k|H|j\rangle = \frac{1}{T}\int_0^T \mathrm{d}t H(t)\exp[-i(j-k)\Omega t]. \tag{21}$$

and we find the Floquet-matrix representation for eq. (19),

$$\sum_{n=1}^{\infty}\sum_{j=-\infty}^{\infty}\langle\varphi_m|\langle k|\mathcal{H}_F|j\rangle|\varphi_n\rangle c_{\alpha,n}^{(j)} = \epsilon_\alpha c_{\alpha,m}^{(k)}, \tag{22}$$

with the Floquet-matrix representation $\mathcal{H}_F$ for $\mathcal{H}$ defined by

$$\langle\varphi_m|\langle k|\mathcal{H}_F|j\rangle|\varphi_n\rangle \equiv \langle\varphi_m|H^{j-k}|\varphi_n\rangle + j\hbar\Omega\delta_{j,k}\delta_{m,n}. \tag{23}$$

To find the quasienergies ϵ_α we therefore have to find the eigenvalues of the Floquet matrix $\mathcal{H}_F$. These eigenvalues are identical to the original time-dependent problem, up to multiples of $\hbar\Omega$. The problem of finding these eigenvalues is therefore reduced to finding the eigenvalues of $\mathcal{H}_F$.
For example, we consider a sinusoidal perturbation with phase ϕ

$$H(t) = H_0 - 2\hbar\lambda\sigma_x\sin(\Omega t + \phi) \tag{24}$$

for one qubit. For one qubit we have $\mathcal{R} = \langle\{|\varphi_0\rangle, |\varphi_1\rangle\}\rangle$ with $|\varphi_0\rangle = |0\rangle$ and $|\varphi_1\rangle = |1\rangle$. In this case, the operator H^{j-k} takes on a triangular structure

$$H^{j-k} = H_0\delta_{j,k} + i\hbar\lambda\sigma_x(\delta_{j,k+1}\exp(i\phi) - \delta_{j,k-1}\exp(-i\phi)) \tag{25}$$

We now set $\hbar = 1$ and since the quasienergies do not depend on the phase ϕ, we set $\phi = 0$. With that, H^{j-k} simplifies to

$$H^{j-k} = H_0\delta_{j,k} + i\lambda\sigma_x(\delta_{j,k+1} - \delta_{j,k-1}) \tag{26}$$

and the operator $\mathcal{H}_F$ can be written as

$$\mathcal{H}_F = H_0 \otimes S_0 + \lambda(\sigma_x \otimes S_y) + \Omega(\mathbb{1} \otimes S_z), \tag{27}$$

where the operators S_0, S_y and S_z acting on $\mathcal{T}$ are defined by

$$\begin{aligned}
\langle k|S_0|j\rangle &\equiv \delta_{j,k} \\
\langle k|S_x|j\rangle &\equiv \delta_{j,k+1} + \delta_{j,k-1} \\
\langle k|S_y|j\rangle &\equiv i\delta_{j,k+1} - i\delta_{j,k-1} \\
\langle k|S_z|j\rangle &\equiv j\delta_{j,k}.
\end{aligned} \tag{28}$$

We additionally defined the operator S_x, which will be used later. The operators S_0, S_x, S_y, S_z have the properties of spin-operators on a subspace of $\mathcal{T}$, up to prefactors. The quasienergies can now be derived from the eigenvalues of $\mathcal{H}_F$, namely $\epsilon_{\alpha,j}$, obeying the periodicity conditions

$$\epsilon_{\alpha,j} = \epsilon_{\alpha,0} + j\Omega. \tag{29}$$

With this, we now have to solve an eigenvalue problem on an extended Hilbert space. However, due to the exponentially scaling Hilbert space, this is a difficult problem for a classical computer. Various classical techniques have been employed such as time-dependent dynamical mean-field theory [12], time-dependent density matrix renormalization group [13], kinetic equations [14], perturbative high-frequency expansions [15], and exact diagonalization [16], but most of them are either not universally applicable or scale exponentially in system size [6].
In the next section, we therefore look at a way to tackle this problem using a variational quantum algorithm.

2.2 Variational quantum algorithms

In the last section we ended up with an eigenvalue problem on an extended Hilbert space. To treat it, we employ a hybrid quantum-classical algorithm, namely a variational quantum algorithm (VQA). This type of algorithm is designed to utilize both quantum and classical resources to find approximate solutions to eigenvalue and optimization problems not accessible to classical computers. In this section we first explain the working principle of a variational quantum algorithm. Then we describe a special case of a VQA, namely the variational quantum eigensolver (VQE). We follow the introduction to variational quantum algorithms from [10].
A schematic of the workings of a variational quantum algorithm can be seen in fig. 1. First we define a cost function $C(\vec{\theta})$ depending on a set of parameters $\vec{\theta}$, which we want to optimize. We have to be able to get the cost function efficiently by performing measurements on the quantum computer, otherwise there would be no potential speed-up over classical alternatives. We then use the quantum computer only to evaluate $C(\vec{\theta})$ for a certain set of parameters. These are updated by the classical optimizer, using a classical optimization procedure to find the minimal argument of the cost function $\arg\min_\theta C(\vec{\theta})$. The end result is a set of parameters $\vec{\theta}_{\min}$ which minimizes $C(\vec{\theta})$.

2.2.1 Algorithm outline

The variational quantum algorithm can be outlined in the following way:

(1) Prepare the ansatz state $|\Psi(\vec{\theta})\rangle$ on the quantum computer, where $\vec{\theta}$ can be any adjustable parameter set. In general, the state $|\Psi(\vec{\theta})\rangle$ is prepared through application of a unitary gate sequence $U(\vec{\theta})$ such that

$$|\Psi(\vec{\theta})\rangle = U(\vec{\theta})|\vec{0}\rangle, \tag{30}$$

where $|\vec{0}\rangle$ denotes some computational basis state.

(2) Measure the cost function $C(\vec{\theta}) = C(|\Psi(\vec{\theta})\rangle)$.

(3) Use a classical optimization algorithm to determine new values of $\vec{\theta}$ that decrease $C(\vec{\theta})$.

(4) Iterate this procedure until convergence in $C(\vec{\theta})$. The final parameters $\vec{\theta}$ define the desired state. This state will be the best possible approximation of the state $|\Psi(\vec{\theta})\rangle$ that minimizes $C(|\Psi(\vec{\theta})\rangle)$ achievable in the set $\{|\Psi(\vec{\theta})\rangle\}_{\vec{\theta}\in I}$.

We first describe the variational principle as the foundation for the variational quantum eigensolver, which is a variational quantum algorithm specifically for finding ground states of a quantum system. After that, we explain the specific algorithm used in this work, which can be seen as an extension of the VQE.

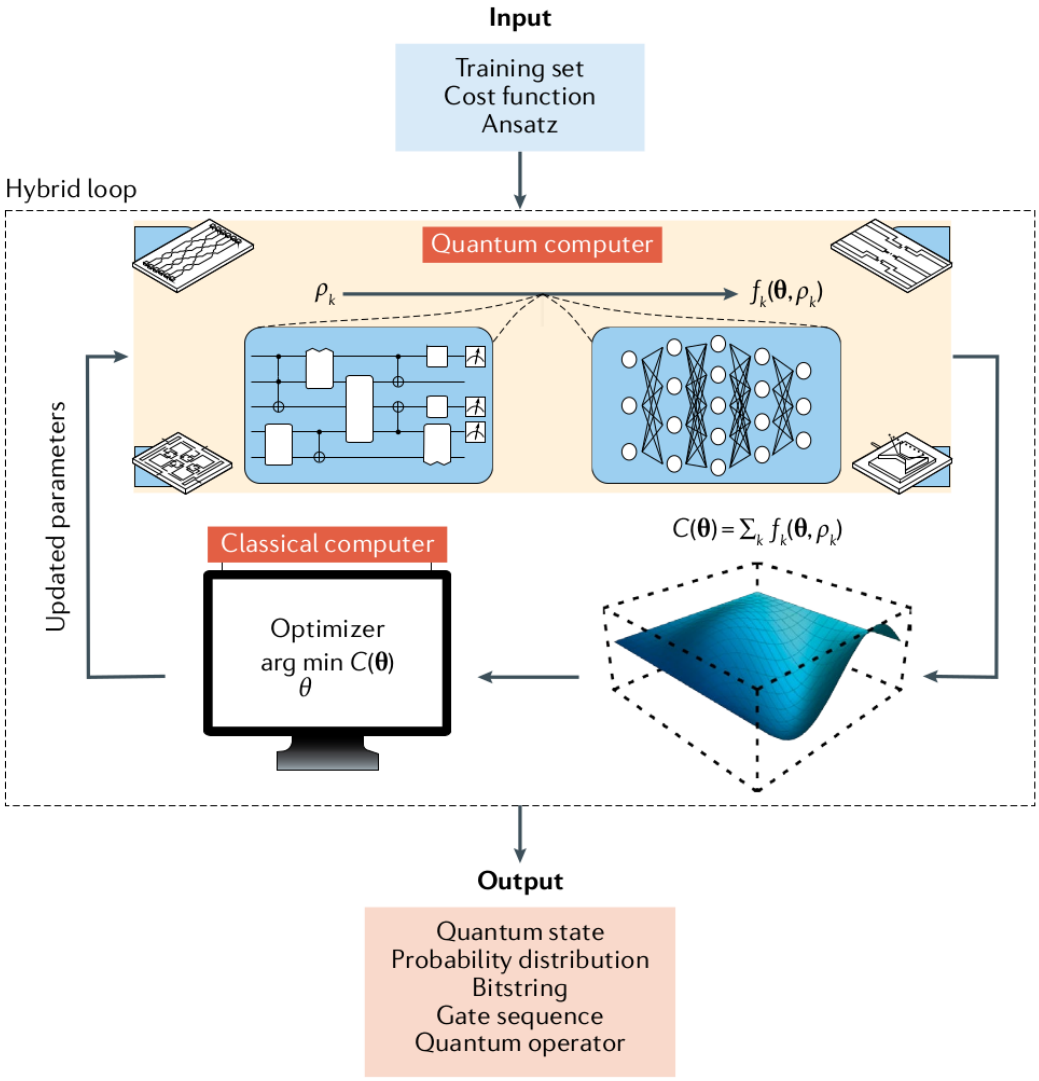

Figure 1: Schematic diagram of a variational quantum algorithm, taken from [10]. The VQA consists of a quantum computer and a classical computer. On the quantum computer, a parametrized circuit is applied to calculate functions depending on the parameters $\vec{\theta}$. Optionally, these functions can be dependent on a set of training data $\{\rho_k\}$, which can be used to improve the algorithm itself. The calculated values are used to compute the cost function $C(\vec{\theta})$. A classical computer optimizes this cost function and returns the minimal argument $\arg\min_\theta C(\vec{\theta})$.

2.2.2 The variational principle

Let us consider a quantum computer S composed of N qubits, and a Hamiltonian H of a system Q of which we want to find the ground state $|\xi_1\rangle$ and the ground state eigenvalue λ_1. We furthermore order the eigenvalues such that $\lambda_1 \leq \lambda_2 \leq \cdots \leq \lambda_N$.
Recall that the expectation value of an operator O with respect to a state $|\psi\rangle$ is given by

$$\langle O \rangle_{|\psi\rangle} = \langle \psi | O | \psi \rangle \tag{31}$$

We consider only the class of operators whose expectation value can be measured efficiently on S and mapped to Q. A sufficient condition is that operators have a decomposition into

a polynomial sum of simple operators as

$$O = \sum_{\alpha} h_\alpha O_\alpha \tag{32}$$

where O is an operator that acts on Q and each O_α has a simple measurement prescription on the system S. We can therefore determine the expectation values of O on Q by weighted summation of projective measurements on the quantum device S.
The core ingredient of variational quantum computing is the variational principle. Suppose we have a Hamiltonian on the system Q, whose mapping to S we call H. The variational principle states that for a multi-parameter family of normalized states $\{\Psi(\vec{\theta})\}_{\vec{\theta}\in I}$, it holds for all $\vec{\theta}$ that

$$\langle H\rangle_{|\Psi(\vec{\theta})\rangle} \equiv \langle H\rangle(\vec{\theta}) = \langle\Psi(\vec{\theta})|H|\Psi(\vec{\theta})\rangle \geq \lambda_1. \tag{33}$$

The elements $\vec{\theta}$ of I are vectors which represent sets of real valued parameters $\{\theta_i\}$ that define the parametrized state $\Psi(\vec{\theta})$ on S.
If we therefore find a minimum of $\langle\Psi(\vec{\theta})|H|\Psi(\vec{\theta})\rangle$, we get the closest possible solution to the ground state reachable within the set $\{\Psi(\vec{\theta})\}_{\vec{\theta}\in I}$. To find this minimum, we can now use a variational quantum algorithm as described in the last section, where we use

$$C(\vec{\theta}) = \langle\Psi(\vec{\theta})|H|\Psi(\vec{\theta})\rangle \tag{34}$$

for the cost function.
To find eigenstates and eigenvalues of H we thus have to find the choice of $\vec{\theta}$ which minimizes $\langle H\rangle_{|\Psi(\vec{\theta}\rangle}$.

2.2.3 The ansatz state

For the performance of any variational quantum algorithm, the parametrization of the state $|\psi(\vec{\theta})\rangle$, called the **ansatz**, is of great importance. To retain the possibility of speed-up over classical computers, the number of parameters θ_i should remain relatively small while $|\psi(\vec{\theta})\rangle$ has to be able to reach the ground state of H, or the minimum of $C(\vec{\theta})$, at least approximately. In general, even parametrized quantum circuits will still not be able to represent the ground state exactly [17]. However, they do offer an expressivity advantage compared to classical generative algorithms [18].
Constructing an ansatz for a parametrized quantum circuit is non-trivial in general. There exist several approaches to construct an ansatz for a given VQE or hardware architecture [19, 20]. Later in this work we present possibilities to construct ansatzes based on the Hamiltonian of which we want to find the eigenvalues using a VQE.

2.2.4 Algorithm for treating Floquet dynamics

We now present a specific variational quantum algorithm to find the eigenvalues of the Floquet matrix $\mathcal{H}_F$ defined in eq. (23). The algorithm we present is the Fauseweh-Zhu-2

algorithm from [6].
Written in its Fourier components, $\mathcal{H}_F$ reads

$$\mathcal{H}_F^{j,k} = H^{j-k} - j\Omega\delta_{j,k}, \tag{35}$$

where Ω denotes the driving frequency and $\hbar$ has been set to 1. Note that the operator

$$\mathcal{H}_F = H - \Omega(\mathbb{1} \otimes S_z), \tag{36}$$

with S_z defined as in eq. (28), acts on the extended Hilbert space $\mathcal{R} \otimes \mathcal{T}$. The operators $\mathcal{H}_F^{j,k}$ act on the Hilbert space $\mathcal{R}$. We denote a state of the extended Hilbert space as $|j\rangle|\Psi\rangle$. We furthermore define $N \equiv \dim(\mathcal{R})$.
To find the eigenvalues of $\mathcal{H}_F$, we want to use a variational quantum algorithm. However, since the Fourier space $\mathcal{T}$ is infinite-dimensional, we have to truncate it at $j_{\max}$, so the indices j, k run over $\{-j_{\max}, \ldots, j_{\max}\}$ instead of $\mathbb{Z}$. Thus, the truncated space $\mathcal{T}^{(j_{\max})}$ has dimension $2j_{\max} + 1$. After the truncation the matrix $\mathcal{H}_F$ can be written as

$$\mathcal{H}_F^{(j_{\max})} = H^{(j_{\max})} - \Omega(\mathbb{1}_N \otimes S_z^{(j_{\max})}), \tag{37}$$

where $S_z^{(j_{\max})}$ is the $(2j_{\max} + 1)$-dimensional matrix S_z acting on $\mathcal{T}^{(j_{\max})}$ as defined in eq. (28) for $j, k \in \{-j_{\max}, \ldots, j_{\max}\}$. The matrix $H^{(j_{\max})}$ is defined by its Fourier components $H_{j,k}^{(j_{\max})} = H^{j-k}$ for $j, k \in \{-j_{\max}, \ldots, j_{\max}\}$.
To simplify the following consideration we now switch to a single-index notation for $\mathcal{R} \otimes \mathcal{T}^{(j_{\max})}$, so instead of (n, j), $n \in \{1, \ldots, N\}, j \in \{-j_{\max}, \ldots, j_{\max}\}$ we use l, $l \in \{1, \ldots, (2j_{\max} + 1)N\}$, where the single index $(j_{\max} - j)N + n$ corresponds to the double index (n, j). We now assume that the driving frequency Ω is much larger than the eigenvalues $\{\lambda_l\}_{l\in\{1,\ldots,(2j_{\max}+1)N\}}$ of $H^{(j_{\max})}$ from eq. (37), therefore

$$\lambda_l \ll \Omega. \tag{38}$$

We now order the $(2j_{\max} + 1) \cdot N$ eigenvalues $\{\lambda_l\}_{l\in\{1,\ldots,(2j_{\max}+1)N\}}$ of $H^{(j_{\max})}$ and $\{\gamma_l\}_{l\in\{1,\ldots,(2j_{\max}+1)N\}}$ of $\mathcal{H}_F^{(j_{\max})}$ by

$$\begin{aligned} &\lambda_1 \geq \lambda_2 \geq \cdots \geq \lambda_{(2j_{\max}+1)N} \text{ and} \\ &\gamma_1 \geq \gamma_2 \geq \cdots \geq \gamma_{(2j_{\max}+1)N}. \end{aligned} \tag{39}$$

Note that the ordering of the $\{\lambda_l\}_{l\in\{1,\ldots,(2j_{\max}+1)N\}}$ is not related to the ordering of the $\{\gamma_l\}_{l\in\{1,\ldots,(2j_{\max}+1)N\}}$. We proceed similarly for the eigenvalues $\{\Omega_l\}_{l\in\{1,\ldots,(2j_{\max}+1)N\}}$ of $\Omega(\mathbb{1}_N \otimes S_z^{(j_{\max})})$, such that

$$\Omega_1 \geq \Omega_2 \geq \cdots \geq \Omega_{(2j_{\max}+1)N}. \tag{40}$$

The eigenvalues of $\Omega(\mathbb{1}_N \otimes S_z^{(j_{\max})})$ are $j\Omega$, and each one is N-times degenerate. Therefore,

if we assume the above ordering, then for each $l \in \{1, \ldots, (2j_{\max}+1)N\}$ it holds that

$$\Omega_l = j\Omega \text{ for } l \in M_j = \{(j_{\max} - j)N + 1, \ldots, (j_{\max} - j + 1)N\}, \tag{41}$$

since $j\Omega$ decreases when $j_{\max} - j$ increases and the sets

$$\{M_j = \{(j_{\max} - j)N + 1, \ldots, (j_{\max} - j + 1)N\}\}_{j \in \{-j_{\max}, \ldots, j_{\max}\}} \tag{42}$$

form a partition of $\{1, \ldots, (2j_{\max}+1)N\}$ where each set M_j contains exactly N consecutive indices.
In ref. [21] it has been shown that, given the orderings above, for the eigenvalues $\{\gamma_l\}_{l \in \{1, \ldots, (2j_{\max}+1)N\}}$ of $\mathcal{H}_F^{(j_{\max})}$ from eq. (37), it holds that

$$\max_{\alpha+\beta=(2j_{\max}+1)N+l} \lambda_\alpha + \Omega_\beta \leq \gamma_l \leq \min_{\alpha+\beta=l+1} \lambda_\alpha + \Omega_\beta. \tag{43}$$

Since $\lambda_l \ll \Omega$ and due to eq. (41), we know that for all choices of α_1, α_2 and β_1, β_2 such that

$$\Omega_{\beta_1} < \Omega_{\beta_2} \Leftrightarrow \exists j' \in \{1, \ldots, 2j_{\max}\} : \Omega_{\beta_2} = \Omega_{\beta_1} + j'\Omega \tag{44}$$

it holds that

$$\lambda_{\alpha_1} + \Omega_{\beta_1} < \lambda_{\alpha_2} + \Omega_{\beta_2}. \tag{45}$$

Hence, due to the orderings in eq. (39) and eq. (40), we get that

$$\begin{aligned}
\max_{\alpha+\beta=(2j_{\max}+1)N+l} \lambda_\alpha + \Omega_\beta &= \max_{\{\mu \in \{1, \ldots, (2j_{\max}+1)N\}, \Omega_{l+\mu} = \Omega_l\}} \lambda_{(2j_{\max}+1)N-\mu} + \underbrace{\Omega_{l+\mu}}_{=\Omega_l} \\
&\geq \lambda_{(2j_{\max}+1)N} + \Omega_l \text{ and} \\
\min_{\alpha+\beta=l+1} \lambda_\alpha + \Omega_\beta &= \min_{\{\mu \in \{1, \ldots, (2j_{\max}+1)N\}, \Omega_{l-\mu} = \Omega_l\}} \lambda_{1+\mu} + \underbrace{\Omega_{l-\mu}}_{=\Omega_l} \\
&\leq \lambda_1 + \Omega_l.
\end{aligned} \tag{46}$$

Combined, this gives

$$\lambda_{(2j_{\max}+1)N} + \Omega_l \leq \gamma_l \leq \lambda_1 + \Omega_l. \tag{47}$$

From eq.(41) we now get that

$$\lambda_{(2j_{\max}+1)N} + j\Omega \leq \gamma_l \leq \lambda_1 + j\Omega \text{ for } l \in M_j. \tag{48}$$

For simplicity, we now drop the superscript $j_{\max}$ and write $\mathcal{H}_F$ instead of $\mathcal{H}_F^{(j_{\max})}$ for the truncated operator. Writing $\lambda_{\min} \equiv \lambda_{(2j_{\max}+1)N}$ and $\lambda_{\max} \equiv \lambda_1$ as the minimum and maximum eigenvalues of H and returning to the index notation (n, j), $n \in \{1, \ldots, N\}, j \in$

$\{-j_{\max}, \ldots, j_{\max}\}$, where the double index (n, j) corresponds to the single index $(j_{\max} - j)N + n$, we finally obtain for the eigenvalues

$$\left\{\gamma_{n,j} = \gamma_{(j_{\max}-j)N+n}\right\}_{n\in\{1,\ldots,N\}, j\in\{-j_{\max},\ldots,j_{\max}\}} \tag{49}$$

of $\mathcal{H}_F$ the inequality

$$\lambda_{\min} + j\Omega \leq \gamma_{n,j} \leq \lambda_{\max} + j\Omega. \tag{50}$$

This means that for every $j \in \{-j_{\max}, \ldots, j_{\max}\}$ there are exactly N eigenvalues $\{\gamma_{n,j}\}_{n\in\{1,\ldots,N\}}$ of $\mathcal{H}_F$ with the property

$$\gamma_{n,j} = \lambda_{n,j} + j\Omega \tag{51}$$

with $\lambda_{n,j} \in [\lambda_{\min}, \lambda_{\max}]$ and $\lambda_{n,j} \ll \Omega$. We therefore get a band structure for the eigenvalues of $\mathcal{H}_F^{(j_{\max})}$, where we have one band of N eigenvalues for each value of j.
This means that if we want to get the quasienergies ϵ_α, we have to find the values of $\lambda_{n,j}$. Due to finite-size errors introduced by the truncation these values are only approximations for the ϵ_α. We also have to note here that the $\lambda_{n,j}$ in general are not the same for different j. However, we expect the finite-size errors to be smallest in the center of the band structure, so we want to find only the eigenvalues $\{\lambda_{n,0}\}_{n\in\{0,\ldots,N\}}$. These are the N eigenvalues of $\mathcal{H}_F$ with the lowest absolute value. Therefore, we minimize $\mathcal{H}_F^2$ instead of $\mathcal{H}_F$ to find the eigenstates of $\mathcal{H}_F^2$.
These can then be used to get the corresponding eigenvalues of $\mathcal{H}_F$ by measuring the expectation value of $\mathcal{H}_F$ after optimization. We note here that since we optimize the expectation value of $\mathcal{H}_F^2$, we run into a problem which occurs when the operator $\mathcal{H}_F$ has two eigenvalues λ_1 and λ_2 with $\lambda_1 \neq \lambda_2 \wedge \lambda_1^2 = \lambda_2^2 \Leftrightarrow \lambda_1 = -\lambda_2$. An extension for this algorithm which solves this problem is presented in section 3.1. Using that procedure, we will find the eigenvalue with the lowest absolute value, which makes sure that the eigenvalue lies in the center of the band structure. A graphical interpretation of the procedure is shown in fig. 2.
To find eigenvalues other than just the ground state eigenvalue, we define the cost function to optimize using a Lagrange multiplier to project out the previously computed θ_β.

$$C(\vec{\theta}) = \langle\vec{0}|_{\mathcal{R}}\langle\vec{0}|_{\mathcal{T}} U^\dagger(\vec{\theta})\mathcal{H}_F^2 U(\vec{\theta})|\vec{0}\rangle_{\mathcal{T}}|\vec{0}\rangle_{\mathcal{R}} + \Lambda\sum_\beta \left|\langle\vec{0}|_{\mathcal{R}}\langle\vec{0}|_{\mathcal{T}} U^\dagger(\vec{\theta}_\beta)U(\vec{\theta})|\vec{0}\rangle_{\mathcal{T}}|\vec{0}\rangle_{\mathcal{R}}\right|^2, \tag{52}$$

where we assumed an ansatz state to be the parametrized state given by $|\psi(\vec{\theta})\rangle = U(\vec{\theta})|\vec{0}\rangle_{\mathcal{T}}|\vec{0}\rangle_{\mathcal{R}}$, with the computational basis state $|\vec{0}\rangle_{\mathcal{T}}|\vec{0}\rangle_{\mathcal{R}}$. The Λ-term, with $\Lambda > 0$, prevents us from finding solutions for already obtained eigenvalues by adding the overlap with all previously found solutions as a penalty to the cost function. The algorithm is outlined in alg. (1).
This algorithm benefits from a mixed qudit-qubit architecture, as the truncated part of $\mathcal{T}$ naturally leads to states such as $|\pm j\rangle_{\mathcal{T}}|\varphi\rangle_{\mathcal{R}}$ with $|\varphi\rangle_{\mathcal{R}}$ in $\mathcal{R}$.

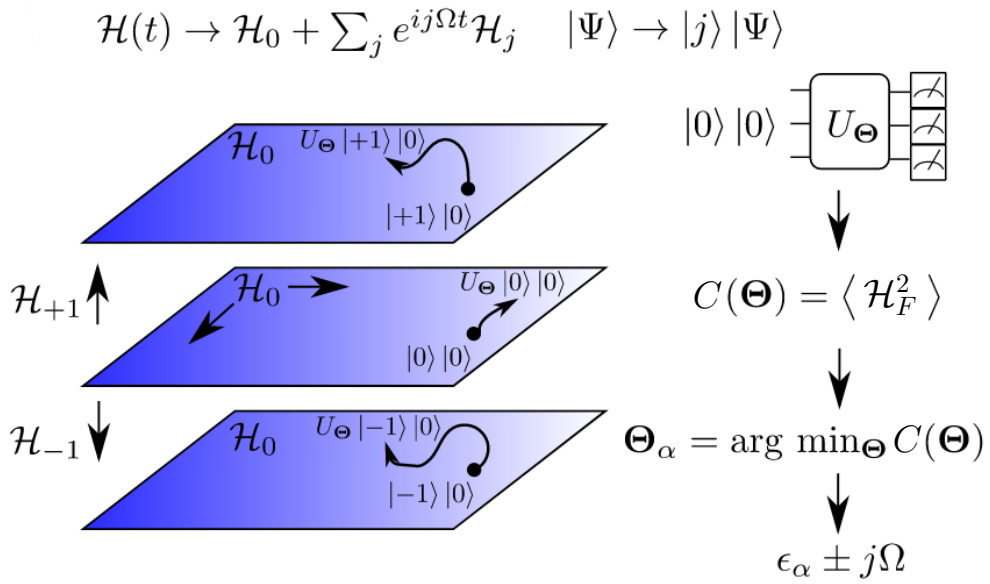

Figure 2: Graphical representation of the algorithm to find the quasienergies ϵ_α, adapted from [6]. The Hilbert space is extended by Fourier expansion of the Hamiltonian. A parametrized quantum circuit then approximated the combined Floquet state described by both physical and Fourier quantum numbers. The operator $\mathcal{H}_0$ acts within one plane, while the operators $\mathcal{H}_j$ introduce hopping in j-direction.

The executability and the speed-up of this algorithm, like with any variational quantum algorithm, depends on the ansatz [19]. We now turn our attention to methods of constructing such an ansatz. We first present a general approach to finding an ansatz for a variational quantum algorithm, which we then use to construct an ansatz for this algorithm in particular.

Algorithm 1 Fauseweh-Zhu-2

Require:
Parametrized quantum circuit $U(\vec{\theta})$ in extended Hilbert space $\mathcal{R} \otimes \mathcal{T}$
Previous solutions $\vec{\theta}_\beta$
Floquet matrix $\mathcal{H}_F$
Truncation value $j_{\max}$
procedure OPTIMIZE($U(\vec{\theta})$)
  Choose initial parameters $\vec{\theta}$
  while Minimize $C(\vec{\theta})$ **do**
    Evaluate observable $\langle\vec{0}|_\mathcal{R}\langle\vec{0}|_\mathcal{T} U^\dagger(\vec{\theta})\mathcal{H}_F^2 U(\vec{\theta})|\vec{0}\rangle_\mathcal{T}|\vec{0}\rangle_\mathcal{R}$
    Evaluate circuits $U^\dagger(\vec{\theta}_\beta)U(\vec{\theta})|\vec{0}\rangle_\mathcal{T}|\vec{0}\rangle_\mathcal{R}$
    Update parameters $\vec{\theta}$ to decrease target $C(\vec{\theta})$
  end while
  Compute $\epsilon_\alpha \pm j\omega = \langle\vec{0}|_\mathcal{R}\langle\vec{0}|_\mathcal{T} U^\dagger(\vec{\theta})\mathcal{H}_F U(\vec{\theta})|\vec{0}\rangle_\mathcal{T}|\vec{0}\rangle_\mathcal{R}$
  return $\epsilon_\alpha \pm j\omega$, $\vec{\theta}_\alpha$
end procedure

2.3 Ansatz construction

As we already mentioned in section 2.2.2, for a variational quantum algorithm the ansatz is of great importance. It determines the possible accuracy of the result and the speed of the algorithm, since the number of parameters affects the runtime of the quantum circuit as well as the convergence behaviour of the optimizer. There exist several approaches to create an ansatz for a VQE. They can be general ansatzes suitable for any problem, or problem-specific ansatzes, i.e. ansatzes tailored to a specific problem. In this section we focus on the problem-specific perturbative ansatz constructed in [22]. There, an ansatz is constructed by a diagrammatic ansatz finding scheme for a given Hamiltonian.
This will help us construct our own ansatz for the Fauseweh-Zhu-2 algorithm. Before we outline the perturbative scheme, we first present an overview of general ansatz construction.

2.3.1 Theoretical basics

We define a variational ansatz on N_p parameters by a pair $(U, |\vec{0}\rangle)$ wih a **starting state** $|\vec{0}\rangle \in \mathcal{C}^{2^{N_q}}$ and a smooth map from the parameter space $\mathcal{R}^{N_p}$ to a unitary operator $U(\vec{\theta})$. The **variational state** to parameters $\vec{\theta}$ of this ansatz is then $|\psi(\vec{\theta})\rangle = U(\vec{\theta})|\vec{0}\rangle$ with variational energy $E(\vec{\theta}) = \langle\psi(\vec{\theta})|H|\psi(\vec{\theta})\rangle$.
We call a variational ansatz $(U, |\vec{0}\rangle)$ a **product ansatz** if the unitary operator $U(\vec{\theta})$ for all $\vec{\theta}$ can be written as

$$U(\vec{\theta}) = \prod_{i=1}^{N_u} U_i(\theta_{n_i}) \tag{53}$$

where each U_i has a generator T_i such that

$$U_i(\theta_{n_i}) = e^{iT_i\theta_{n_i}} \tag{54}$$

A schematic for such an ansatz can be seen in fig. 3.

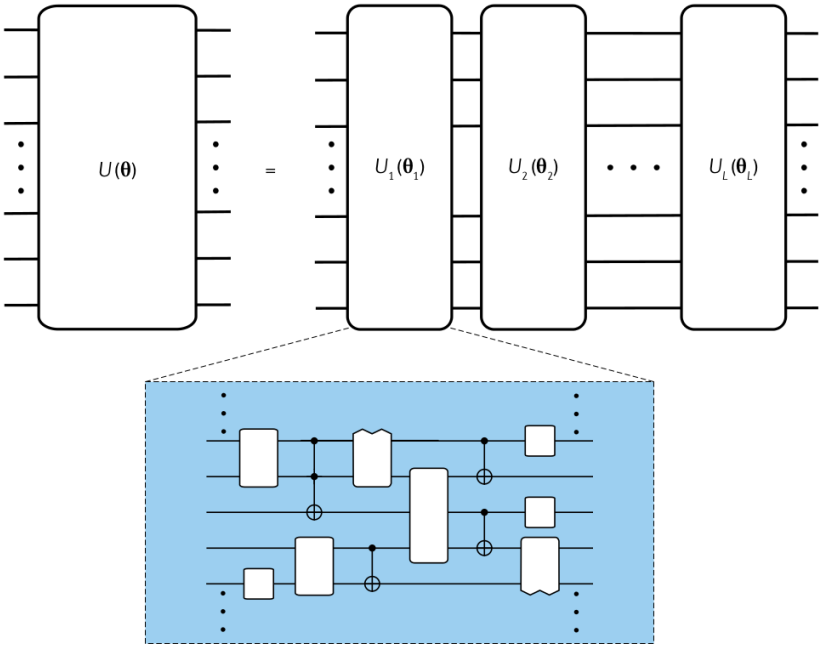

Figure 3: Schematic diagram of a product ansatz, taken from [10]. The unitary $U(\vec{\theta})$, with θ a set of parameters, can be expressed as a product of L unitaries $U_l(\theta_l)$ sequentially acting on an input state $|\vec{0}\rangle$. Each unitary $U_l(\theta_l)$ can in turn be decomposed into a sequence of parametrized and unparametrized gates.

We furthermore call the ansatz **ordered** if $i > j \Rightarrow n_i > n_j$ and a **Pauli-type ansatz** if each generator $T_i \in \mathcal{P}^{N_q} := \{I, X, Y, Z\}^{\otimes N_q}$, where X, Y and Z denote the Pauli-x, y and -z-operators respectively.

2.3.2 Diagrammatic perturbative construction

Now we consider a more complex method for constructing an ansatz proposed in [22]. To explain the construction we first need to state some further definitions. Then, we look into a diagrammatic expansion of the ground state of a Hamiltonian using perturbation theory, which we can use to find an ansatz for the VQE algorithm.
To construct the ansatz we first define an ansatz which spans the whole space, from which we can then construct smaller ansatzes by taking only specific generators. This ansatz, namely the **quantum combinatorial ansatz (QCA)** is defined as an ansatz $(U, |\vec{0}\rangle)$ with

$$U = \prod_{n=1}^{N_q} U^{(n)}, \text{ where } U^{(n)} = \prod_{j=0,1} \prod_{S \in \mathcal{S}^{(n)}} e^{i\theta^n_{S,j} S R^{(n)}_j} \tag{55}$$

with $|s_i\rangle = |\vec{0}\rangle, R^{(n)}_0 = X_n, R^{(n)}_1 = Y_n$ and $\mathcal{S}^{(n)} = \langle X_i, i \in \{1, \ldots, n-1\}\rangle$. The generators of this ansatz are given by $T^n_{S,j} = S R^{(n)}_j$.
We can now look at ansatzes derived from this one. A product ansatz $(U', |\vec{0}'\rangle)$ is called a

child ansatz of a parent product ansatz $(U', |\vec{0}'\rangle)$ if each U_i' of U' also appears in U. Our goal is now to find for a specific Hamiltonian H a child ansatz of the QCA which can get to the ground state of H efficiently.

Construction

To construct this child ansatz we now again apply perturbation theory. For this, we first split the Hamiltonian into a non-interacting part H_0 and a coupling part $JV(\|H_0\|, \|V\| \sim 1)$:

$$H = H_0 + JV \tag{56}$$

We denote the computational basis states by $|\vec{s}\rangle$, which can be expressed in terms of the eigenstates of H_0, namely $|E_j^0\rangle$.
If we try to perform this construction we run into a challenge called "back-action". This describes the fact that the action of a unit $U_i(\theta_i)$ on the state $\prod_{j<i} U_j(\theta_j)|\vec{0}\rangle$ may be very different to the action of $U_i(\theta_i)$ on the starting state. This could potentially generate undesired terms to the variational wavefunction which would then have to be cancelled out by later rotations. It can be shown that the ansatz constructed here automatically cancels out the back-action terms [22].
The construction process is based on the target equality

$$|E_0\rangle \simeq |\psi(\vec{\theta})\rangle, \tag{57}$$

where $|E_0\rangle$ denotes the ground state of the Hamiltonian H and $|\psi(\vec{\theta})\rangle = U(\vec{\theta})|\vec{0}\rangle$ denotes the parametrized state of the ansatz. The construction is based on expanding both sides of this equation in terms of a Pauli decomposition of the perturbation

$$JV = \sum_{i=1}^{N_c} J_i V_i, \quad \text{where } V_i \in \mathbb{P}^{N_q} \tag{58}$$

and equating terms based on the order of their polynomial dependence on each J_i. This can be thought of as a formal way to treat a perturbative ansatz under the assumption that we can decompose the perturbation into products of Pauli matrices. However, this restriction makes this ansatz construction unsuitable for some specific cases, especially for an architecture which also features qudits.

Diagrammatic expansion of the ground state

For the expansion of the ground state $|E_0\rangle$ we use vector notation $\vec{J}$ and $\vec{V}$ for the coupling terms J_i and the operators V_i respectively. We furthermore use the notation

$$\vec{a}^{\vec{k}} \equiv \prod_i a_i^{k_i} \tag{59}$$

With that we can write the expansion of the ground state as a Taylor series in $\vec{J}$

$$|E_0\rangle = \sum_{\vec{k}\in\mathbb{N}^{N_c}} \vec{J}^{\vec{k}}|\psi_{\vec{k}}\rangle, \tag{60}$$

where the $|\psi_{\vec{k}}\rangle$, after a standard Dyson expansion, take the form

$$|\psi_{\vec{k}}\rangle = C_{\vec{k}}\vec{V}^{\vec{k}}|\vec{0}\rangle. \tag{61}$$

We can now assign to each coefficient $C_{\vec{k}}$ a so-called perturbative diagram. First we note that a vector $\vec{V}$ of N_c Pauli operators defines a phase $\Gamma(\vec{k}) \in \{0,1,2,3\}$ and a state $\vec{s}(\vec{k})$ on a vector $\vec{k} \in \mathbb{N}^{N_c}$ by

$$\vec{V}^{\vec{k}}|\vec{0}\rangle = i^{\Gamma(\vec{k})}|\vec{s}(\vec{k})\rangle. \tag{62}$$

For a contribution $C_{\vec{k}}$ we call the set of qubits on which at least one V_i with $k_i \neq 0$ acts non-trivially the **support** of $\vec{k}$. We furthermore say that a contribution $C_{\vec{k}}$ is **disconnected** if one can write $\vec{k} = \vec{k}_A + \vec{k}_B$, where the respective supports of $\vec{k}_A$ and $\vec{k}_B$ do not share any qubits. We can now give the following definition:
Let $\vec{V}$ define the order of a decomposition of the perturbation $\vec{J}\cdot\vec{V}$ to a non-interacting Hamiltonian H_0. A **perturbative diagram** for a vector $\vec{k}$ is defined as a bipartite graph with one circular vertex for each qubit, and k_β square vertices for each interaction V_β. We draw edges between each square vertex and the qubits that the corresponding V_β-term acts non-trivially on, and color the edge to qubit i blue, red or black if $[V_\beta]_i = X, Y$ or Z respectively. Each circular vertex is then colored black or white if it is connected to by an odd or even number of colored edges respectively. Examples for perturbative diagrams are illustrated in fig. (4). We can then read off some properties of this graph:

- A contribution $C_{\vec{k}}$ is connected if all square vertices in the perturbative diagram are connected.
- We can read off $\vec{s}(\vec{k})$ off the graph by setting $\vec{s}_i(\vec{k}) = 0$ when the corresponding circular vertex is white and $\vec{s}_i(\vec{k}) = 1$ otherwise.
- Since the red lines represent Y-operators, we can read off $\Gamma(\vec{k}) \mod 2$ as being the number of red lines modulo 2.

We can now perform a Taylor expansion of the variational ansatz $U(\vec{\theta})$ and compare the terms based on the order of their polynomial dependence on each J_i. We find that for a child ansatz derived from the QCA to be able to find the ground state of H, the only generators we need to consider are those generators $T_{\vec{s}(\vec{k}),a(\vec{k})}$, where $a(\vec{k}) := \Gamma(\vec{k}) \mod 2$ and $T_{\vec{s},a}$ is defined by

$$iT_{\vec{s},a}|\vec{0}\rangle = i^a|\vec{s}\rangle. \tag{63}$$

We can find all generators with nonzero coefficients by constructing the perturbative

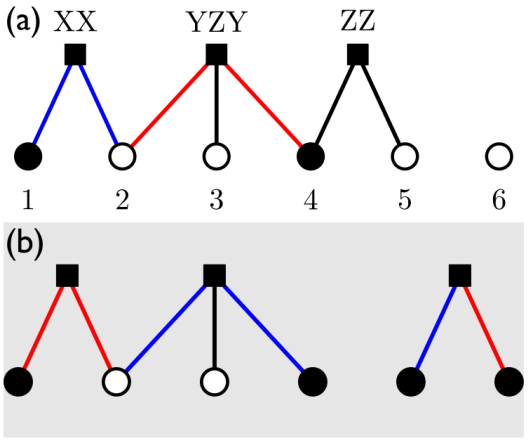

Figure 4: Example for perturbative diagrams, taken from [22]. An example for a connected diagram for a real contribution to $\vec{s}(\vec{k}) = |100100\rangle$ with labels for qubits i and terms V_β is given by (a). In (b) we see a disconnected diagram for an imaginary contribution to $\vec{s}(\vec{k}) = |100111\rangle$.

diagrams associated to each $\vec{k}$. We then can impose a condition on the perturbative diagrams which tells us if $T_{\vec{s}(\vec{k}),a(\vec{k})}$ has to be a generator of the final ansatz. We first define what it means for a connected perturbative diagrams to be **sub-leading** to another one. We call a diagram D for a vector $\vec{k}$ sub-leading to a diagram D' for a vector k' if

- D and D' have identically colored vertices, implying $\vec{s}(\vec{k}) = \vec{s}(\vec{k}')$.
- D and D' have the same number of red edges modulo 2, implying $a(\vec{k}) = a(\vec{k}')$.
- D' has fewer interaction vertices than D, implying $|\vec{k}| < |\vec{k}'|$

We then call a diagram **leading** with respect to a set of diagrams P if it is not a sub-leading diagram to any other $D' \in P$.
The condition for $T_{\vec{s}(\vec{k}),a(\vec{k})}$ to be a generator of the ansatz is now that the associated perturbative diagram is connected and leading [22]. Furthermore we can even define an order on the generators by $|\vec{k}|_1 = \sum_i |k_i|$ of the contribution, which gives us the order in J of the prefactor of the contribution in eq. (60). These conditions now can be used to find an implementable rule for constructing this ansatz.

Example: spin-chain

We demonstrate the diagrammatic construction of this ansatz by considering the example of the one-dimensional transverse-field Ising model. Its Hamiltonian is given by

$$H_{\text{TFIM}} = -\sum_{i=1}^{N_q} hZ_i + \sum_{i=1}^{N_q-1} JX_iX_{i+1}. \tag{64}$$

We now construct all the connected leading perturbative diagrams for the TFIM with $N_q = 4$, illustrated in fig. 5.

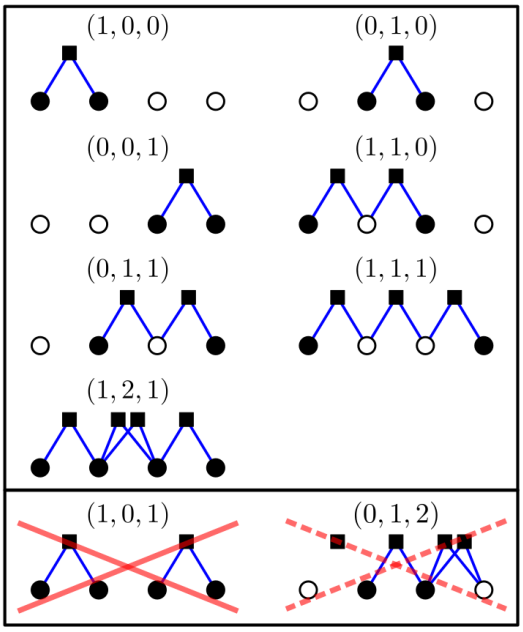

Figure 5: The seven lowest order leading diagrams for the four-site TFIM, labeled by their associated $\vec{k}$. Depicted at the bottom are examples of diagrams which do not need to be considered. At the bottom left we see a disconnected diagram, and the diagram at the bottom right is sub-leading of the $\vec{k} = (0, 1, 0)$-diagram above. Figure taken from [22].

From the diagrams we can then read off the generators for the variational ansatz. They are given by taking X_i operators for the respective black circles until the last one, for which we take Y_i if the number of red lines is even and X_i if it is odd. We get

$$\begin{aligned} &T_1 = X_1Y_2,\ T_2 = X_2Y_3,\ T_3 = X_3Y_4, \\ &T_4 = X_1Y_3,\ T_5 = X_2Y_4,\ T_6 = X_1Y_4, \\ &T_7 = X_1X_2X_3Y_4 \end{aligned} \tag{65}$$

We can now order the generators corresponding to their order in J, giving

- 3 contributions at order J (to T_1, T_2 and T_3)
- 2 contributions at order J^2 (to T_4, and T_5)
- 1 contribution at order J^3 (to T_6)
- 1 contribution at order J^4 (to T_7)

which finally gives us a guess for the ordering of the perturbative terms. The final ansatz for the $N_q = 4$ spin-chain then reads $(U, |\vec{0}\rangle)$,where

$$U(\vec{\theta}) = \prod_{i=1}^{7} \exp(i\theta_j T_j). \tag{66}$$

and $|\vec{0}\rangle = |0\rangle^{\otimes 4}$.

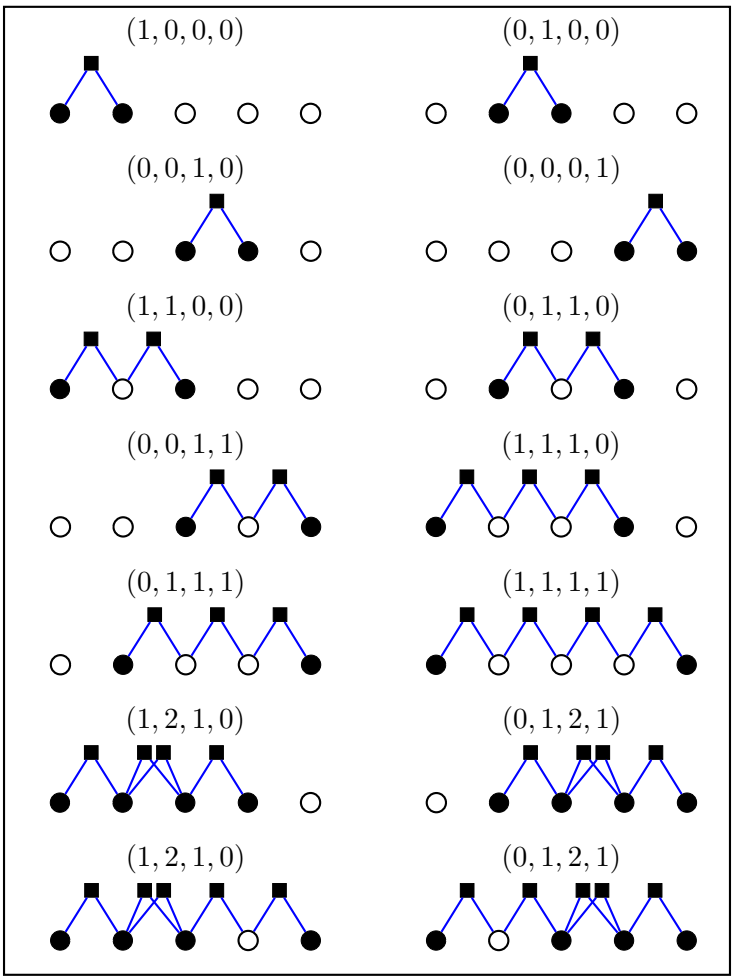

Figure 6: The lowest order diagrams for the five-site TFIM. All the diagrams for the four-site TFIM are represented, plus additional ones exclusive to the five-site TFIM.

For comparison, we also give the generators for the $N_q = 5$ spin-chain, generated by the perturbative diagrams depicted in figure 6. In this case, we have twice as many diagrams as in the case of $N_q = 4$. The generators then read

$$\begin{aligned} T_1 &= X_1Y_2,\ T_2 = X_2Y_3,\ T_3 = X_3Y_4, \\ T_4 &= X_4Y_5,\ T_5 = X_1Y_3,\ T_6 = X_2Y_4, \\ T_7 &= X_3Y_5,\ T_8 = X_1Y_4,\ T_9 = X_2Y_5, \\ T_{10} &= X_1Y_5,\ T_{11} = X_1X_2X_3Y_4, \\ T_{12} &= X_2X_3X_4Y_5,\ T_{13} = X_1X_2X_3Y_5, \\ T_{14} &= X_1X_3X_4Y_5. \end{aligned} \tag{67}$$

2.3.3 General ansatz

To compare to the ansatz constructed later by combining this diagrammatic method with another more naive method, we also implemented a general, not problem-specific ansatz for n qubits and a qudit with 3 states. For this ansatz, we choose $|\vec{0}\rangle = |0\rangle^{\otimes n} \otimes |1\rangle_{\text{qd}}$, where

$|1\rangle_{\text{qd}}$ is the eigenstate of S_z corresponding to eigenvalue 1 on the qudit. We construct the general ansatz as $(U_g, |\vec{0}\rangle)$ with

$$U_g(\vec{\theta}) = \prod_{d=1}^{D} \Bigg[\prod_{j=1}^{n} e^{i\theta_j^{(1,d)} Z_j \otimes \mathbb{1}} \prod_{j=1}^{n} e^{i\theta_j^{(2,d)} Y_j \otimes \mathbb{1}} \prod_{j=1}^{n} e^{i\theta_j^{(3,d)} Z_j \otimes \mathbb{1}} \times \\ \times \prod_{j=1}^{n} \left(\prod_{l=j}^{n} e^{i\theta_{jl}^{(4,d)} X_j X_l \otimes \mathbb{1}} \right) \prod_{k=1}^{8} e^{i\theta_k^{(5,d)} \mathbb{1} \otimes G_k} \prod_{j=1}^{n} e^{i\theta_j^{(6,d)} X_j \otimes S_z} \Bigg], \tag{68}$$

where D denotes the depth of the circuit and $\{G_k\}_{k \in \{n \in \mathbb{N}, n \leq 8\}}$ is the set of Gell-Mann matrices:

$$G_1 = \begin{pmatrix} 0 & 1 & 0 \\ 1 & 0 & 0 \\ 0 & 0 & 0 \end{pmatrix}, \quad G_2 = \begin{pmatrix} 0 & -i & 0 \\ i & 0 & 0 \\ 0 & 0 & 0 \end{pmatrix}, \quad G_3 = \begin{pmatrix} 1 & 0 & 0 \\ 0 & -1 & 0 \\ 0 & 0 & 0 \end{pmatrix}, \\ G_4 = \begin{pmatrix} 0 & 0 & 1 \\ 0 & 0 & 0 \\ 1 & 0 & 0 \end{pmatrix}, \quad G_5 = \begin{pmatrix} 0 & 0 & -i \\ 0 & 0 & 0 \\ i & 0 & 0 \end{pmatrix}, \\ G_6 = \begin{pmatrix} 0 & 0 & 0 \\ 0 & 0 & 1 \\ 0 & 1 & 0 \end{pmatrix}, \quad G_7 = \begin{pmatrix} 0 & 0 & 0 \\ 0 & 0 & -i \\ 0 & i & 0 \end{pmatrix}, \quad G_8 = \frac{1}{\sqrt{3}} \begin{pmatrix} 1 & 0 & 0 \\ 0 & 1 & 0 \\ 0 & 0 & -2 \end{pmatrix}. \tag{69}$$

3 Algorithm Construction

We now propose a way to improve the Fauseweh-Zhu-2 algorithm presented in section 2.2.4 and find an efficient ansatz for it. In section 3.1, we explain an extension for the algorithm which solves an issue we run into when faced with degeneration in the eigenvalues of the Floquet matrix $\mathcal{H}_F$. Then we focus on constructing the ansatz for the algorithm. In section 3.3 we present a naive ansatz construction method which is less efficient but more generally applicable than the diagrammatic method presented in section 2.3.2. We then explain a way to combine both those ansatz schemes to obtain a problem-specific ansatz for a mixed qubit-qudit architecture in section 3.4. This combined ansatz construction scheme is the one we evaluate in section 4 for the Fauseweh-Zhu-2 algorithm.

3.1 Extending the algorithm

In section 2.2.4 we explained the Fauseweh-Zhu-2 algorithm. For this algorithm, we search for eigenstates of $\mathcal{H}_F^2$ and then get the eigenvalues of $\mathcal{H}_F$ in the center of the band structure by taking the expectation value of $\mathcal{H}_F$. This means that we run into a problem which occurs when the operator $\mathcal{H}_F$ has two eigenvalues λ_1 and λ_2 with

$$\lambda_1 \neq \lambda_2 \wedge \lambda_1^2 = \lambda_2^2 \Leftrightarrow \lambda_1 = -\lambda_2. \tag{70}$$

In this case, the algorithm will find any vector in the span $\langle|\psi_1\rangle, |\psi_2\rangle\rangle$, where $|\psi_1\rangle$ and $|\psi_2\rangle$ denote the eigenvectors to the eigenvalues λ_1 and λ_2, respectively. This means that the eigenvectors $|\psi_1'\rangle = U(\vec{\theta}_1)|\vec{0}\rangle_{\mathcal{T}}|\vec{0}\rangle_{\mathcal{R}}$ and $|\psi_2'\rangle = U(\vec{\theta}_2)|\vec{0}\rangle_{\mathcal{T}}|\vec{0}\rangle_{\mathcal{R}}$ we get from the algorithm can differ from the eigenvectors $|\psi_1\rangle$ and $|\psi_2\rangle$ of $\mathcal{H}_F$ in this case, which can lead to great errors in the approximated eigenvalues of $\mathcal{H}_F$. To correct for this, we have to do another step of the algorithm which finds those incorrect eigenvectors and corrects them by optimizing again. However, we have to restrict our optimization to the eigenspace $\langle|\psi_1\rangle, |\psi_2\rangle\rangle = \langle|\psi_1'\rangle, |\psi_2'\rangle\rangle$. This can be achieved by subtracting the overlap with the subspace from the cost function. To find the eigenvectors of $\mathcal{H}_F$ which differ from those of $\mathcal{H}_F^2$, it is useful to not directly minimize $\langle\vec{0}|_{\mathcal{R}}\langle\vec{0}|_{\mathcal{T}}U^\dagger(\vec{\theta})\mathcal{H}_F U(\vec{\theta})|\vec{0}\rangle_{\mathcal{T}}|\vec{0}\rangle_{\mathcal{R}}$, but rather minimize the variance

$$\mathrm{Var}(\mathcal{H}_F) = \langle\vec{0}|_{\mathcal{R}}\langle\vec{0}|_{\mathcal{T}}U^\dagger(\vec{\theta})\mathcal{H}_F^2 U(\vec{\theta})|\vec{0}\rangle_{\mathcal{T}}|\vec{0}\rangle_{\mathcal{R}} - \Big(\langle\vec{0}|_{\mathcal{R}}\langle\vec{0}|_{\mathcal{T}}U^\dagger(\vec{\theta})\mathcal{H}_F U(\vec{\theta})|\vec{0}\rangle_{\mathcal{T}}|\vec{0}\rangle_{\mathcal{R}}\Big)^2. \tag{71}$$

We get for the modified cost function

$$C^{(1)}_{\langle|\psi_1\rangle,|\psi_2\rangle\rangle}(\vec{\theta}) = \mathrm{Var}(\mathcal{H}_F) - \Lambda_2 \sum_{i=1}^{2} \Big|\langle\psi_i'|U(\vec{\theta})|\vec{0}\rangle_{\mathcal{T}}|\vec{0}\rangle_{\mathcal{R}}\Big|^2. \tag{72}$$

If our ansatz can reach an eigenstate of $\mathcal{H}_F$ on $\langle|\psi_1\rangle, |\psi_2\rangle\rangle$, the minimum of the $\mathrm{Var}(\mathcal{H}_F)$ should always be 0. This means that, if we choose Λ_2 to be large enough, the minimal argument of this function will always be some $\vec{\theta}$ with $U(\vec{\theta})|\vec{0}\rangle_{\mathcal{T}}|\vec{0}\rangle_{\mathcal{R}} \in \langle|\psi_1\rangle, |\psi_2\rangle\rangle$. By optimizing $C_{\langle|\psi_1\rangle,|\psi_2\rangle\rangle}(\vec{\theta})$ and finding the solution $\vec{\theta}_0$, we therefore get an eigenvector of

$\mathcal{H}_F$ on $\langle|\psi_1\rangle, |\psi_2\rangle\rangle$. If we now want to find the second eigenvector of $\mathcal{H}_F$ on $\langle|\psi_1\rangle, |\psi_2\rangle\rangle$, we simply have to add the overlap with the previously found solution again as in eq. (52). This gives

$$C^{(2)}_{\langle|\psi_1\rangle,|\psi_2\rangle\rangle}(\vec{\theta}) = \mathrm{Var}(\mathcal{H}_F) + \Lambda_1 \left|\langle\vec{0}|_{\mathcal{R}}\langle\vec{0}|_{\mathcal{T}} U^\dagger(\vec{\theta}_1) U(\vec{\theta})|\vec{0}\rangle_{\mathcal{T}}|\vec{0}\rangle_{\mathcal{R}}\right|^2 - \Lambda_2 \sum_{i=1}^{2} \left|\langle\psi_i'|U(\vec{\theta})|\vec{0}\rangle_{\mathcal{T}}|\vec{0}\rangle_{\mathcal{R}}\right|^2. \tag{73}$$

With this, we now can construct a two-step algorithm, where in the first step we find the eigenvectors of $\mathcal{H}_F^2$ and then in the second step, we search for eigenvectors $|\psi_1\rangle$, $|\psi_2\rangle$ with eigenvalues λ_1, λ_2 which fulfill eq. (70) and optimize $C^{(1)}_{\langle|\psi_1\rangle,|\psi_2\rangle\rangle}(\vec{\theta})$ and $C^{(2)}_{\langle|\psi_1\rangle,|\psi_2\rangle\rangle}(\vec{\theta})$ to find the correct eigenvectors of $\mathcal{H}_F$ on $\langle|\psi_1\rangle, |\psi_2\rangle\rangle$.

3.2 Algorithm for the diagrammatic ansatz construction

In this thesis, the perturbative construction from section 2.3.2 is used to create ansatzes for the algorithm outlined in section 2.2.4 for different systems. For this purpose we created and implemented the algorithm presented in alg. 2 to find the generators $\{T_i\}$ for an ansatz for a given Pauli decomposition of a Hamiltonian.

Algorithm 2 Pseudocode for perturbative ansatz construction

Require:
Decomposition of H into l products of Pauli matrices and number of qubits N_Q
List K of all k-vectors of length l with $|k|_1 < N_Q$ and sorted by absolute value
procedure FIND ALL RELEVANT DIAGRAMS(K)
For every k-vector, generate associated perturbative diagram to get list P of perturbative diagrams.
Perturbative diagram has methods to get $s(\vec{k})$, get number of edges, find if it is disconnected and create associated T-operator.
for p in P **do**
if p is leading w.r.t. P and p not disconnected (per definition in sec. 2.3.2) **then**
if $s(p) \neq 0$ **then**
Store p in list P'.
end if
end if
end for
end procedure
Generate all the generators $\{T_i\}$ from the list P' of perturbative diagrams.

3.3 Naive perturbative ansatz construction

We now consider a naive approach to finding an ansatz based on perturbation theory. This simple approach is not efficient for larger systems of qubits, but is a very general approach which works for any architecture. Therefore, this approach is applicable for single qudits, which can be used in combination with the more complicated, size-extensive perturbative construction explained in the section 2.3.2 to treat mixed qubit-qudit architectures.

We consider a product ansatz with generators A_i. We now want to use perturbation theory to find some set of matrices such that the ansatz can "reach" all of the eigenstates of H. We first consider a Hamiltonian consisting of a diagonal and a nondiagonal part

$$H = H_0 + H_{ND} = H_D + JV. \tag{74}$$

The nondiagonal part is assumed to be small ($J \ll 1$), so that we can consider JV as small perturbation. Let $|E_n^0\rangle$, $n \in I$ denote the eigenstates of the unperturbed Hamiltonian H_0, which in our case are just the basis vectors of the Hilbert space. We then get for the first order correction in perturbation theory with degeneracy that

$$\left|E_n^0\right\rangle = \sum_{k \notin D_n} \frac{\langle E_k^0|V|E_n^0\rangle}{E_n - E_k}\left|E_k^0\right\rangle, \tag{75}$$

where $D_n = \{k \in I, E_n = E_k\}$ denotes a possibly degenerate eigenspace.
We now want to find the required generators A_i for a product ansatz. In the following we assume that we already have a partial ansatz of the same form which is able to get all the eigenstates of H_0 out of one starting state $|\vec{0}\rangle$, e.g.

$$\left|E_n^0\right\rangle = \prod_{j \in I_D} e^{i\theta_j A_j}|\vec{0}\rangle, \tag{76}$$

where I_D is a subset of the actual index set of the final ansatz. This means that we already can reach all the eigenstates of H_0 with a part of the ansatz, so we focus only on finding the part of the ansatz that considers the nondiagonal part of the Hamiltonian. For this purpose we again look at eq. (75). The eigenstates in first order perturbation theory have the form

$$|E_n\rangle = \left|E_n^0\right\rangle + \sum_{k \notin D_n} \frac{\langle E_k^0|V|E_n^0\rangle}{E_n - E_k}\left|E_k^0\right\rangle. \tag{77}$$

This means that to encompass the states $|E_n\rangle$ in our ansatz, it has to be able to change between states $|E_n^0\rangle$ and $|E_k^0\rangle$ if $\langle E_k^0|V|E_n^0\rangle \neq 0$. A reasonable approach to find this ansatz would therefore be to look at all the nonzero elements of V, which are just all the $\langle E_k^0|V|E_n^0\rangle \neq 0$, since H_0 is diagonal, and then include in the ansatz some operators which can change between those states.

Transitioning between states

We now have a condition for an ansatz to be able to reach all possible eigenstates. The ansatz has to include operators which can transition between specific states given the matrix elements of the perturbation operator in the eigenbasis of H_0. We now have to find generators that create operators able to transition between specific eigenstates of H_0. We first look at the simple case of a two-state system and then extend the method to a general system.

2-state system

We first consider the simple case of a two-level system. In this case, we only have two states, $|0\rangle$ and $|1\rangle$ with $Z|0\rangle = |0\rangle$ and $Z|1\rangle = -|1\rangle$. We can describe any pure state of this system using the Bloch-sphere, e.g.

$$|\psi\rangle = \cos\left(\frac{\theta}{2}\right)|0\rangle + e^{i\phi}\sin\left(\frac{\theta}{2}\right)|1\rangle. \tag{78}$$

We can rotate between these states using the rotation matrices $e^{-i\theta A}$, where $A \in \{X, Y, Z\}$, to rotate in the different rotational bases of the Bloch-sphere.

Rotating between general states

Now we can apply this principle of rotating between states on our system. If we want to rotate between two states $|E_n^0\rangle$ and $|E_k^0\rangle$, we first find some operator $A_z^{(nk)}$ with $A_z^{(nk)}|E_n^0\rangle = |E_n^0\rangle$ and $A_z^{(nk)}|E_k^0\rangle = -|E_k^0\rangle$. This operator is easy to find in our case, because H_D is diagonal. We therefore have that

$$\left(A_z^{(nk)}\right)_{ij} = \delta_{in}\delta_{jn} - \delta_{ik}\delta_{jk}. \tag{79}$$

To apply the same procedure as in the previous example, we have to find $A_x^{(nk)}$ and $A_y^{(nk)}$ with the same commutation relations to $A_z^{(nk)}$ as the X, Y to Z, so we can construct the rotation operators like in the last section. We can define the $A_x^{(nk)}$, $A_y^{(nk)}$ as

$$\left(A_x^{(nk)}\right)_{ij} \equiv \delta_{in}\delta_{jk} + \delta_{ik}\delta_{jn} \text{ and } \left(A_y^{(nk)}\right)_{ij} \equiv i(\delta_{in}\delta_{jk} - \delta_{ik}\delta_{jn}). \tag{80}$$

We can rotate between the two states by using $e^{-i\theta A_i^{(nk)}}$, $i \in \{x, y\}$. Which of $A_x^{(nk)}$ or $A_y^{(nk)}$ we need is dependent on whether the actual state we want to transition to or from is imaginary or real. If it is imaginary, we need $A_x^{(nk)}$. If it is real, we need $A_y^{(nk)}$. If it is neither imaginary nor real, we need both.

Example: linear-driven spin-$\frac{1}{2}$

We now look at an example for this naive ansatz construction, namely for the linear driven spin-$\frac{1}{2}$. The time-dependent Hamiltonian is given by

$$H(t) = -\frac{\Delta}{2}Z + \frac{A}{2}\sin(\omega t)X \tag{81}$$

The Floquet matrix as in eq. (27) is then given by

$$\mathcal{H}_F = \underbrace{\omega(S_z \otimes \mathbb{1}) - \Delta(\mathbb{1} \otimes Z)}_{H_D} + A\underbrace{(S_y \otimes X)}_{V}, \tag{82}$$

where we truncate the Hilbert space at $j_{\max} = 1$ as explained in section 2.2.4, such that

$$S_x = \begin{pmatrix} 0 & 1 & 0 \\ 1 & 0 & 1 \\ 0 & 1 & 0 \end{pmatrix},\ S_y = \begin{pmatrix} 0 & i & 0 \\ -i & 0 & i \\ 0 & -i & 0 \end{pmatrix},\ S_z = \begin{pmatrix} 1 & 0 & 0 \\ 0 & 0 & 0 \\ 0 & 0 & -1 \end{pmatrix} \tag{83}$$

We now want to find the ansatz to find the Eigenvalues of this operator. We use the Method presented in this section, assuming ω is large, so we can apply perturbation theory.
For that we have to look at the matrix

$$(S_y \otimes X) = \begin{pmatrix} 0 & 0 & 0 & i & 0 & 0 \\ 0 & 0 & i & 0 & 0 & 0 \\ 0 & -i & 0 & 0 & 0 & i \\ -i & 0 & 0 & 0 & i & 0 \\ 0 & 0 & 0 & -i & 0 & 0 \\ 0 & 0 & -i & 0 & 0 & 0 \end{pmatrix}, \tag{84}$$

which consists of the only nondiagonal elements of $\mathcal{H}_F$. We now see that in the upper triangular matrix, only V_{14}, V_{23}, V_{36} and V_{45} are nonzero. Since they are all imaginary, we have to take the $A_x^{(nk)}$ to form our ansatz:

$$A_x^{(23)} = \begin{pmatrix} 0 & 0 & 0 & 0 & 0 & 0 \\ 0 & 0 & 1 & 0 & 0 & 0 \\ 0 & 1 & 0 & 0 & 0 & 0 \\ 0 & 0 & 0 & 0 & 0 & 0 \\ 0 & 0 & 0 & 0 & 0 & 0 \\ 0 & 0 & 0 & 0 & 0 & 0 \end{pmatrix}, A_x^{(14)} = \begin{pmatrix} 0 & 0 & 0 & 1 & 0 & 0 \\ 0 & 0 & 0 & 0 & 0 & 0 \\ 0 & 0 & 0 & 0 & 0 & 0 \\ 1 & 0 & 0 & 0 & 0 & 0 \\ 0 & 0 & 0 & 0 & 0 & 0 \\ 0 & 0 & 0 & 0 & 0 & 0 \end{pmatrix}, \tag{85}$$

$$A_x^{(45)} = \begin{pmatrix} 0 & 0 & 0 & 0 & 0 & 0 \\ 0 & 0 & 0 & 0 & 0 & 0 \\ 0 & 0 & 0 & 0 & 0 & 0 \\ 0 & 0 & 0 & 0 & 1 & 0 \\ 0 & 0 & 0 & 1 & 0 & 0 \\ 0 & 0 & 0 & 0 & 0 & 0 \end{pmatrix}, A_x^{(36)} = \begin{pmatrix} 0 & 0 & 0 & 0 & 0 & 0 \\ 0 & 0 & 0 & 0 & 0 & 0 \\ 0 & 0 & 0 & 0 & 0 & 1 \\ 0 & 0 & 0 & 0 & 0 & 0 \\ 0 & 0 & 0 & 0 & 0 & 0 \\ 0 & 0 & 1 & 0 & 0 & 0 \end{pmatrix} \tag{86}$$

These matrices, together with the matrices $\mathbb{1} \otimes Y$, $S_4 \otimes \mathbb{1}$ and $S_5 \otimes \mathbb{1}$ with

$$S_4 = \begin{pmatrix} 0 & 0 & 0 \\ 0 & 0 & 1 \\ 0 & 1 & 0 \end{pmatrix} \text{ and } S_5 = \begin{pmatrix} 0 & 1 & 0 \\ 1 & 0 & 0 \\ 0 & 0 & 0 \end{pmatrix} \tag{87}$$

which we need to reach the eigenvalues of the unperturbed Hamiltonian, now can be used as generators for an ansatz to calculate the eigenvalues of H. The difficulty with this approach is that the ansatz we obtain consists only of general matrices which are potentially hard to implement on a multi-qubit quantum computer. Furthermore, since the number of nondiagonal matrix elements in the Hamiltonian can scale quadratic in system size, the

number of parameters for the ansatz can get very large, potentially negating the speedup achieved by using quantum resources. Therefore, in the next section we present a more applicable method to find an ansatz for a given Hamiltonian.

3.4 Combination of the construction methods

In section 2.3.2 and section 3.3, we presented two possibilities for constructing an ansatz for a variational quantum algorithm using perturbation theory. The method from section 3.3 is in principle universally applicable, but it generally requires a very large parameter space. The method presented in section 2.3.2 requires significantly less operators, but it cannot always be applied, since it needs the target Hamiltonian to decompose into Pauli operators, which is not always the case, e.g. in the case of qudit-qubit architectures where the qudit has more that two basis states. For the Fauseweh-Zhu-2 algorithm presented in section 2.2.4, which benefits from a mixed qudit-qubit architecture, it therefore could be reasoned that a combination of the two construction methods can be used to obtain an ansatz. In this section we propose a method to combine those methods to obtain a problem-specific ansatz for a mixed qubit-qudit architecture. In the following, we call this ansatz the **combined ansatz**. This is the method we apply to the Fauseweh-Zhu-2 algorithm and evaluate in section 4.

Method

For combining the construction methods we first decompose the Hamiltonian into three parts, one part acting only on the qubit system, one part acting only on the qudit and one interaction part acting on the qudit and the qubit system. We write

$$H = H_{\text{qb}} + H_{\text{qd}} + H_{\text{int}} \tag{88}$$

with

$$H_{\text{int}} = \sum_{k \in K} H_k^{(\text{qb})} \otimes H_k^{(\text{qd})} \tag{89}$$

for some index set K. If we consider the Floquet matrix method presented in section 2.1.2 and assume that the time-dependent perturbations are always cosine or sine, we always have $H_k^{(\text{qd})} \in \{S_x, S_y\}$.
We now construct our ansatz by the following three steps:

(1) First, use the diagrammatic construction to construct an ansatz from H_{qb} given by the generators $\{A_i\}_{i \in I}$.

(2) Now use the naive method to construct an ansatz from H_{qd} and all $H_j^{(\text{qd})}$ occurring in the Hamiltonian, given by the generators $\{B_j\}_{j \in J}$.

(3) Finally, use the diagrammatic construction again to find an ansatz from the interaction term. Since this construction depends on the decomposition of the

Hamiltonian into Pauli-matrices, it does not work for the qudit, which has more than two basis states. However, if we replace the Pauli-matrices for the qudit by S_x, S_y and S_z respectively, we can implement this construction with a qudit. We can then consider the qudit the same way we would an additional qubit. The diagrammatic construction method stays the same. We get the generators $\{C_k\}_{k\in K}$.

For the final ansatz we then get $(U, |\vec{0}\rangle)$ with

$$U(\vec{\theta}) = \prod_l e^{i\theta_l^{(1)} A_l \otimes \mathbb{1}} \prod_j e^{i\theta_j^{(2)} \mathbb{1} \otimes B_j} \prod_{d=1}^{D} \left(\prod_k e^{i\theta_k^{(1,d)} C_k} \prod_l e^{i\theta_l^{(2,d)} A_l \otimes \mathbb{1}} \prod_j e^{i\theta_j^{(3,d)} \mathbb{1} \otimes B_j} \right), \quad (90)$$

where D is the depth of the algorithm. We choose $|\vec{0}\rangle = |0\rangle^{\otimes n} \otimes |0\rangle_{\text{qd}}$, where n is the number of qubits and $|0\rangle_{\text{qd}}$ is the eigenstate of S_z corresponding to eigenvalue 0 on the qudit.

Example

We consider a spin-chain of length 4. The Hamiltonian of a spin-chain of length N_q is given by

$$H_{\text{chain}} = -\sum_{i=1}^{N_q} hZ_i + \sum_{i=1}^{N_q-1} (J_x X_i X_{i+1} + J_y Y_i Y_{i+1} + J_z Z_i Z_{i+1}), \quad (91)$$

with the coupling coefficients J_x, J_y and J_z.
We assume the time-dependent term as

$$A\left(\left(\sum_{i=0}^{N_q} X_i \right) \cos(\Omega t) + \left(\sum_{i=0}^{N_q} Y_i \right) \sin(\Omega t) \right) \quad (92)$$

and we truncate at $j_{\max} = 1$. We can now construct the Floquet operator $\mathcal{H}_F$ like in eq. (35). We get

$$\mathcal{H}_F = \overbrace{-\sum_{i=1}^{N_q} hZ_i + \sum_{i=0}^{N_q-1} (J_x X_i X_{i+1} + J_y Y_i Y_{i+1} + J_z Z_i Z_{i+1})}^{H_{\text{qb}}} + \underbrace{\Omega S_z}_{H_{\text{qd}}} + \underbrace{A\left(\left(\sum_{i=0}^{N_q} X_i \right) \otimes S_x + \left(\sum_{i=0}^{N_q} Y_i \right) \otimes S_y \right)}_{H_{\text{int}}}. \quad (93)$$

Now we go through the steps of the construction.

(1) First, we use the diagrammatic approach to obtain the generators for H_{qd}. All generators we get for $\sum Y_i Y_j$ and $\sum Z_i Z_j$ are already contained in the set of generators obtained for $\sum X_i X_j$. Therefore, we can get all the generators for the diagrammatic ansatz using only $\sum X_i X_j$ as perturbation. This is exactly the example

we already constructed in section 2.3.2. This means we have as generators the operators

$$\{A_i\}_{i\in I} = \{X_1Y_2,\ X_2Y_3,\ X_3Y_4,\ X_1Y_3,\ X_2Y_4,\ X_1Y_4,\ X_1X_2X_3Y_4\}. \tag{94}$$

(2) We use the naive method to construct the ansatz for

$$S_x = \begin{pmatrix} 0 & 1 & 0 \\ 1 & 0 & 1 \\ 0 & 1 & 0 \end{pmatrix} \text{ and } S_y = \begin{pmatrix} 0 & i & 0 \\ -i & 0 & i \\ 0 & -i & 0 \end{pmatrix}. \tag{95}$$

In the same way as in section 3.3 we get the matrices

$$\begin{aligned} B_1 = A_y^{(12)} = \begin{pmatrix} 0 & i & 0 \\ -i & 0 & 0 \\ 0 & 0 & 0 \end{pmatrix},\ B_2 = A_y^{(23)} = \begin{pmatrix} 0 & 0 & 0 \\ 0 & 0 & i \\ 0 & -i & 0 \end{pmatrix} \\ B_3 = A_x^{(12)} = \begin{pmatrix} 0 & 1 & 0 \\ 1 & 0 & 0 \\ 0 & 0 & 0 \end{pmatrix},\ B_4 = A_x^{(23)} = \begin{pmatrix} 0 & 0 & 0 \\ 0 & 0 & 1 \\ 0 & 1 & 0 \end{pmatrix} \end{aligned} \tag{96}$$

In the construction we assumed that we already can rotate between the eigenvalues of the unperturbed Hamiltonian $\Omega S_z = H_{\text{qd}}$, so normally we would have to add further matrices. However, B_3 and B_4 can already rotate between all the eigenstates of S_z, so the matrices

$$\{B_j\}_{j\in J} = \{B_1, B_2, B_3, B_4\} \tag{97}$$

are sufficient.

(3) For the interaction term we now consider

$$H_{\text{int}} = A\left(\left(\sum_{i=0}^{3} X_i\right) \otimes S_x + \left(\sum_{i=0}^{3} Y_i\right) \otimes S_y\right). \tag{98}$$

For the construction, we replace S_x by σ_x and S_y by σ_y and construct the ansatz for the qubit part with an additional qubit. This means we have 5 qubits in total. We then can apply the construction method the same way we did before. Note that we can get generators from this construction that are already contained in $\{A_i\}_{i\in I}$. These can be taken out of this part, because they are already contained in the ansatz.

After removing all the terms we already have in $\{A_i\}_{i\in I}$, we get

$$\{C_k\}_{k\in K} = \{X_4Y_5,\ X_3Y_5,\ X_2Y_5,\ X_2X_3X_4Y_5,\ X_1Y_5,\ X_1X_3X_4Y_5,\ X_1X_2X_3Y_5\}. \tag{99}$$

From these three sets we get an ansatz, depending on circuit depth, as in eq. (90).

4 Numerical Results

In this section we show the results of an explicit implementation of the Fauseweh-Zhu-2 algorithm presented in section 2.2.4. We focus on evaluating the combined ansatz construction from section 3.4 as a way to construct an ansatz for the algorithm. Recall that we call the ansatz obtained using this scheme the **combined ansatz**.
First, we briefly outline the system used for the evaluation and its parameters. We then explain how the algorithm was implemented in section 4.1. In section 4.2, we show the relevance of the two-step algorithm explained in section 3.1 by comparing the algorithm with and without the second step. Following that, we move to evaluating the ansatz construction scheme by comparing an implementation of the algorithm with the combined ansatz to an implementation of the algorithm with the **general ansatz** presented in section 2.3.3.
The system we use for the evaluation is the spin-chain. Its Hamiltonian is given by

$$H_{\text{chain}} = -\sum_{i=1}^{N_q} hZ_i + \sum_{i=1}^{N_q-1} (J_x X_i X_{i+1} + J_y Y_i Y_{i+1} + J_z Z_i Z_{i+1}), \tag{100}$$

with N_q being the chain length and J_x, J_y, J_z the coupling coefficients.
For the time-dependent external field we take

$$A\left(\left(\sum_{i=0}^{N_q} X_i\right)\cos(\Omega t) + \left(\sum_{i=0}^{N_q} Y_i\right)\sin(\Omega t)\right), \tag{101}$$

where A denotes the amplitude of the external field and Ω denotes the driving frequency. We can now construct the Floquet operator $\mathcal{H}_F$. Since the single-qubit operators Z_i are irrelevant for the perturbative diagrams, we leave these operators out of $\mathcal{H}_F$ for the purposes of evaluating the ansatzes. For simplicity, here we furthermore choose $J_x = J_y = J_z = K$. For a truncation value of $j_{\max} = 1$, we then get, as in eq. (93), that

$$\begin{aligned}\mathcal{H}_F = &\left(\sum_{i=0}^{N_q-1} K(X_i X_{i+1} + Y_i Y_{i+1} + Z_i Z_{i+1})\right) + \\ &\Omega S_z + A\left(\left(\sum_{i=0}^{N_q} X_i\right)\otimes S_x + \left(\sum_{i=0}^{N_q} Y_i\right)\otimes S_y\right)\end{aligned} \tag{102}$$

For all further implementations we set the coupling coefficient to $K = 1$ and the driving frequency to $\Omega = 10$.

4.1 Numerical methods

We first explain the method by which the results presented in the following section were obtained. To implement the combined ansatz for a given system Hamiltonian, the steps from section 3.4 were implemented in a c++-program. We additionally used a python program which implements the algorithm from section 3.2 to get the diagrammatic ansatz

for the respective Hamiltonians required and saves them to be read out by the c++-program. The c++-program then implements the complete algorithm outlined in section 2.2.4. It provides the possibility to use either the previously implemented combined ansatz or the general ansatz for an execution of the algorithm.
For the optimizer we used the "bfgs2"-optimizer, which is a gradient-based optimizer [23] from the c++-library gsl [24]. The components of the required gradient of an ansatz state of the form $e^{i\theta_1 T_1} \dots e^{i\theta_N T_N}|\vec{0}\rangle$, where $(T_i)_{i\in\{1,\dots,N\}}$ are the generators, were calculated using the formula

$$\left(\vec{\nabla}\left(e^{i\theta_1 T_1} \dots e^{i\theta_N T_N}|\vec{0}\rangle\right)\right)_i = e^{i\theta_1 T_1} \dots iT_i e^{i\theta_i T_i} \dots e^{i\theta_N T_N}|\vec{0}\rangle. \tag{103}$$

The gradient for the entire cost function $C(\vec{\theta})$ in eq. (52) was then obtained by applying the product rule.
We used two stopping conditions for the optimizer. For the first 100 iterations, the only stopping condition is that the gradient of the function is below a value of 10^{-3}. This condition alone, however, in some cases lead to a high convergence time. For this reason, after the first 100 iterations, the optimizer will also stop when the difference between its current function value and the previous one is below 10^{-7}. The choice of these values is purely for practicality, ensuring adequate accuracy while still having acceptable runtimes.
We executed the program for spin-chains of length 3, 4 and 5. First, the combined ansatz was used, as described in section 3.4. Then, as comparison, the general ansatz, as described in section 2.3.3 was used. The algorithm was run for all depths in the set $\{n \in \mathbb{N}, n \leq 8\}$ for each chain length. One execution of the algorithm for a given chain length, depth and ansatz choice consists of choosing a starting value A_0 for the amplitude A of the external field and calculating the approximated eigenvalues for this value and then increasing this value by an increment δA and calculating the eigenvalues for the next value of A. We repeat this for a predefined number N of steps, such that we get solutions $\{\vec{\theta}_i\}_{i\in\{0,\dots,N\}}$ for all values of A in the set $\{A_i = A_0 + i \cdot \delta A\}_{i\in\{0,\dots,N\}}$. As starting values for the parameters $\vec{\theta}_0^{(0)}$ of the optimizer at A_0, we used random values in the interval $(0, 2\pi)$. Inside each execution of the algorithm, the starting values for the next iteration are then chosen as the calculated values of the previous iteration, i.e. if we got the parameters $\vec{\theta}_i$ for $A = A_i$ as solution of the optimizer, for the next value $A_{i+1} = A_i + \delta A$ we choose the starting values $\vec{\theta}_{i+1}^{(0)}$ as the previous values $\vec{\theta}_i$. If the overlap term in the cost function in eq. (52) is higher than a threshold, the optimization procedure is repeated, where this time the starting values are chosen from a neighbourhood of the previous solution $\vec{\theta}_0$. This means that only the starting parameters at $A = A_0$ were chosen at random.
All the operators and states were implemented as matrices and vectors. For the matrix operations we used the c++-library Eigen. The resulting eigenvalues $\left\{E_k^{(A,\text{calc})}\right\}_{k\in\{1,\dots,N_e\}}$ of $\mathcal{H}_F$ for each value of A, where N_e denotes the number of eigenvalues calculated, were then saved for further evaluation. This was done by a python program, which calculated the normalized sum of the absolute difference of the calculated eigenvalues to the exact ones calculated directly from the matrix using the scipy package. The calculated quantity

for a given value A is then given by

$$D_A = \frac{1}{N_e} \sum_{k=1}^{N_e} \left| E_k^{(A,\text{calc})} - E_k^{(A,\text{exact})} \right|. \tag{104}$$

In all the following examples, N_e was chosen to be the number of eigenvalues in the first Brillouin zone, given by $N_e = 2^{N_q}$, where N_q denotes the chain length. The values $E_k^{(A,\text{calc})}$ and $E_k^{(A,\text{exact})}$ denote the calculated and exact eigenvalues for a given amplitude A, respectively.
Furthermore, for all the examples, we repeat the algorithm for 5 random starting values for the optimizer at the starting value A_0 and take the results where the sum over all differences $\sum_A D_A$ is minimal as final results.
The runtime of this algorithm was generally very high, ranging from hours at chain length 3 to weeks at chain length 5. The order of magnitude of the runtime for each chain length considered is depicted in table 1. The high increase in runtime can be explained with the increase in the number of operators and the quadratic scaling of matrix dimension with system size, i.e. Hilbert space dimension. This observation further underlines the relevance of choosing the ansatz as small as possible, given that reducing the number of operators in the ansatz reduces the time needed to calculate the parametrized state for a given parameter set.

Chain length	Runtime
3	multiple hours
4	multiple days
5	multiple weeks

Table 1: Orders of magnitude for the runtimes of the algorithm for the considered chain lengths.

4.2 Two-step algorithm

To show the relevance of the second step of the algorithm proposed in section 3.1, we first test the algorithm with and without the second step for a chain length of $N_q = 3$ and using the general ansatz defined in eq. (68). To evaluate the algorithm we first calculate the exact eigenvalues of $\mathcal{H}_F$. We then calculate the sum of the differences of the eigenvalues as shown in eq. (104). We plot the inverse of the difference D_A against the amplitude A. To see the dependency of the accuracy of the results on the depth, we plot this for all depth values in $\{n \in \mathbb{N}, n \leq 8\}$. We can see that the accuracy of the calculated eigenvalues dramatically decreases with increasing A. We can create the same plot, this time using the two-step algorithm from section 2.2.4. Both plots are shown in figure 7. Comparing these plots, we see very well that the second step of the algorithm increases the accuracy of the eigenvalues by multiple orders of magnitude, especially for higher A. The dependency of A is presumably due to the fact that the eigenvalues which are degenerate in $\mathcal{H}_F^2$ but not in $\mathcal{H}_F$ are further apart for higher values of A. For $A = 0$, the concerned eigenvalues are

0, so they are degenerate in $\mathcal{H}_F^2$ and $\mathcal{H}_F$, which implies that the second step should not lead to any increase in accuracy. This explains the high accuracy even without the second step for $A = 0$ and the increasing improvement due to the second step with increasing A.

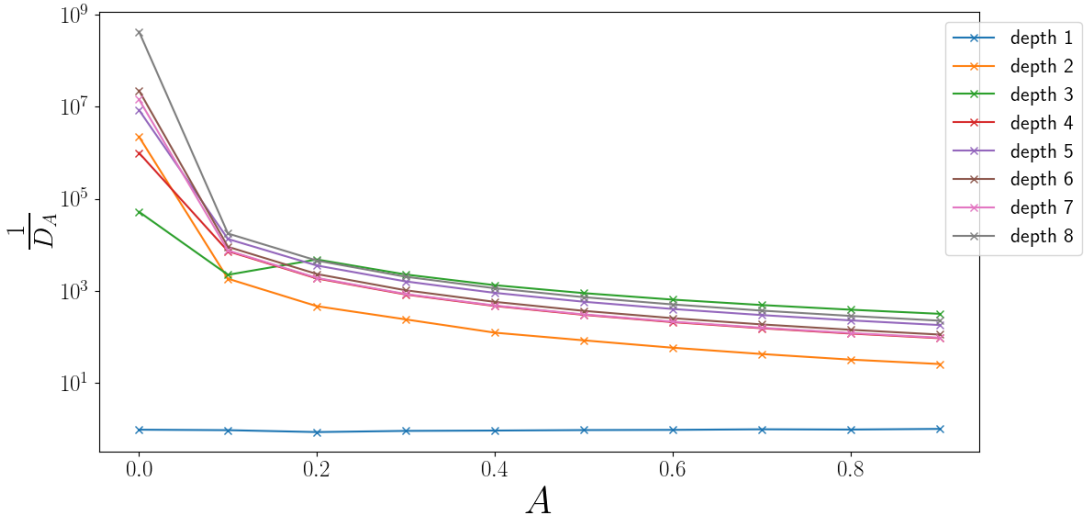

(a) Difference plot without the second step

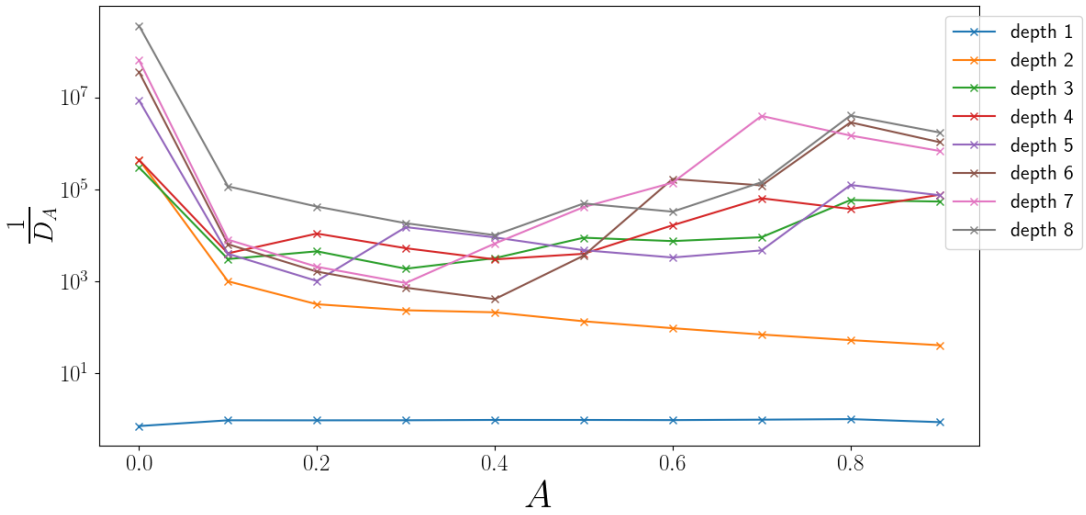

(b) Difference plot with the second step

Figure 7: Comparison of the algorithm with and without the second step for a chain length of 3. In both cases, we used the generic ansatz. As we can see, for larger amplitude A of the external field there is quite a high increase in accuracy due to the introduction of the second step.

4.3 Comparison of ansatz schemes

We now look at the actual results of running the program described above. We consider chain lengths of 3, 4 and 5. For a chain length of 3 and 4 we executed the algorithm once for a starting value of $A_0 = 0$ with a stepwise increase of $\delta A = 0.1$ and once for a starting

value of $A_0 = 1$ with a stepwise increase of $\delta A = 0.5$, in each case with 10 steps. For a chain length of 5 we only executed the algorithm for $A_0 = 1$ with a stepwise increase of $\delta A = 0.5$, since the runtime was already very high in this case. All the executions of the algorithm were done once using the combined ansatz and once using the general ansatz.

Chain length 3

First, we consider a chain length of 3. We repeat the same procedure as in the previous section for the general ansatzand for the combined ansatz.We again plot the difference sum D_A against A for all depth values in $\{n \in \mathbb{N}, n \leq 8\}$. The results are shown in figures 8 and 9.

As we can see, for the general ansatz, it takes a higher depth for the difference to be in the same order of magnitude than for the combined ansatz. One interesting thing to note, however, is that the combined ansatz performs really badly for the case of $A = 0$. The reason for this is unclear, however, since the combined ansatz was constructed using the perturbation term, this could explain why it performs badly in its absence. Another explanation could be that in the case of $A = 0$, some eingenvalues are degenerate in $\mathcal{H}_F$. Since the second step of the algorithm only looks for two degenerate eigenvalues id $\mathcal{H}_F^2$ which are not degenerate in $\mathcal{H}_F$, it could restrict the subsequent search for eigenvectors of $\mathcal{H}_F$ on the wrong subspaces, leading to high errors in the eigenvalues.

Despite this, we can see that, for a nonzero A, the required number of parameters to reach a given proximity to the real eigenvalues is much smaller in the case of the combined ansatz, since we need a lower depth to get to the same proximity. For the combined ansatz we only need a depth of 2 to get to roughly the same proximity, for which we need a depth of 3 with the general ansatz. The number of parameters depending on the depth is shown in table 2. We see that even the number of parameters at the same depths are smaller for the combined ansatz. We have to note, however, that after that, the accuracy of the general ansatz increases still with increasing depth, while in the case of the combined ansatz it stays roughly the same.

Depth	Combined ansatz	General ansatz
1	18	23
2	29	46
3	40	69
4	51	92
5	62	115
6	73	138
7	84	161
8	95	184

Table 2: Number of parameters depending on depth of the combined ansatz and the general ansatz for a chain length of 3.

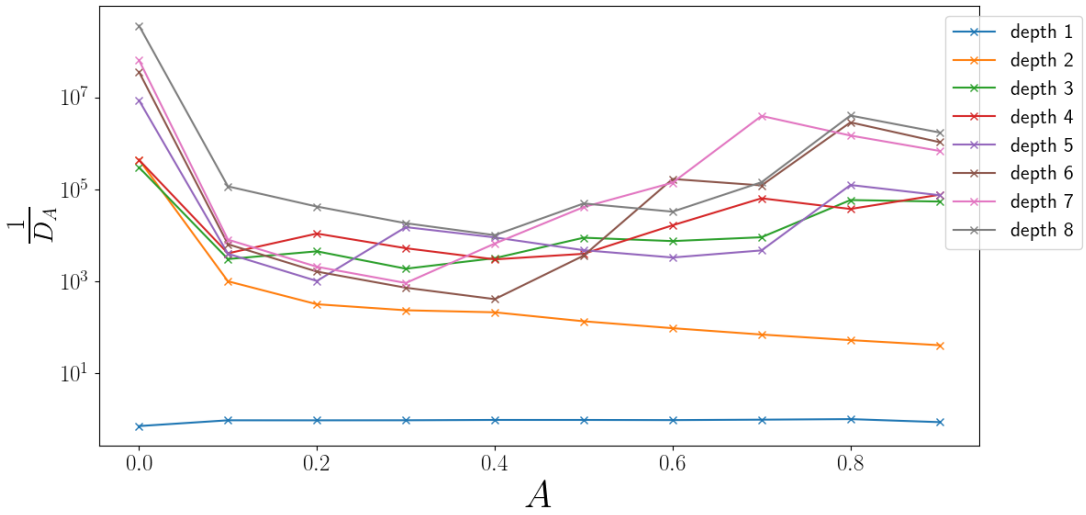

(a) General ansatz

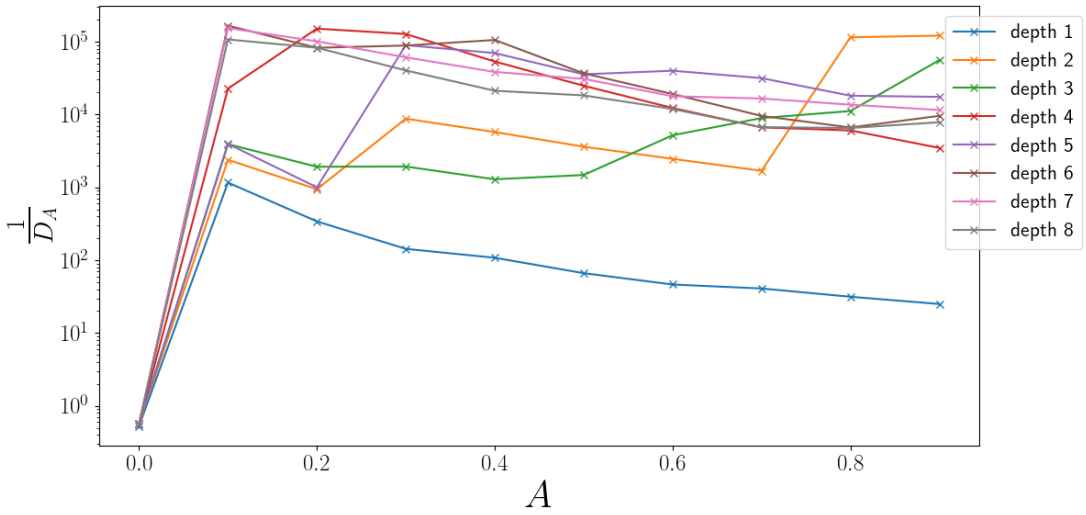

(b) Combined ansatz

Figure 8: Comparison of the combined ansatz and the general ansatz for a chain length of 3 and an initial external field amplitude $A = 0$ with a stepwise increase of 0.1. The plots show that the combined ansatz reaches a higher accuracy with lower depth. We also see very clearly that for $A = 0$, the combined ansatz completely fails, as opposed to the general one.

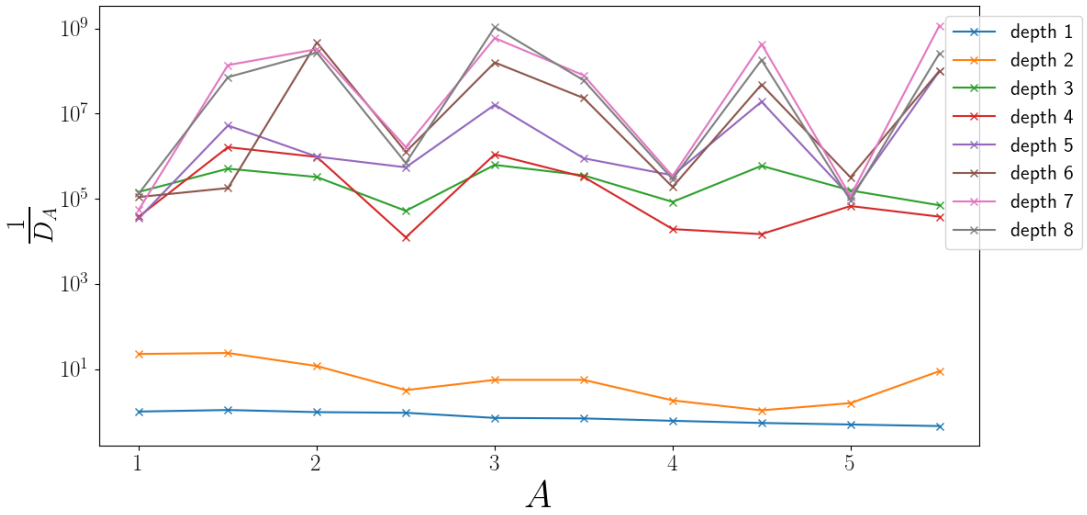

(a) General ansatz

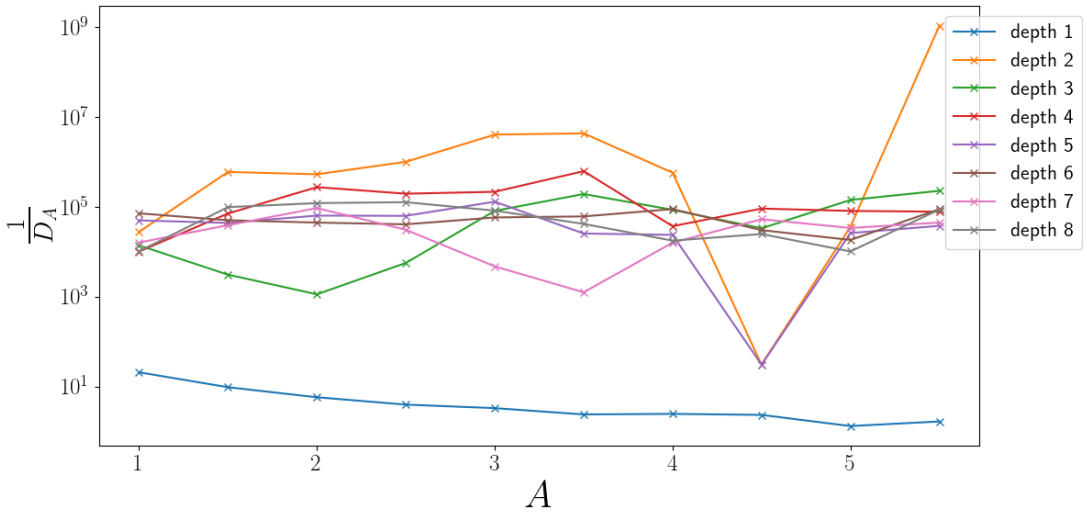

(b) Combined ansatz

Figure 9: Comparison of the combined ansatz and the general ansatz for a chain length of 3 and an initial external field amplitude $A = 1$ with a stepwise increase of 0.5. We see that for higher A, the combined ansatz still reaches higher accuracy with lower depths, but we also see that the maximum accuracy achievable seems to be with the general ansatz at much higher depths.

Chain length 4

We now consider a chain length of 4. The resulting plots are shown in figures 10 and 11. We can make very similar observations to the case of chain length 3. We see that to get to the same accuracy we can reach with a depth of 2 of the combined ansatz, we already need a depth of 5 of the general ansatz. This increase in depth to get a good approximation of the eigenstates corresponds to already confirmed results about depth-dependency of ansatzes for a VQE [25]. Interestingly, for the combined ansatz, it seems that even depth 2 could already be enough to get a good approximation, as it was in the case of a chain length of 3. This suggests a much lower depth scaling for the combined ansatz. The number of parameters needed is therefore again much higher for the general ansatz, as seen in table 3.

As we already saw in the case of chain length 3, the minimum difference value we get for the general ansatz is at $\approx 10^{-7}$. Since we stopped the optimizer at a function value difference of 10^{-7}, this is also the expected difference value for an ansatz that could potentially reach all the eigenstates exactly. For the combined ansatz, we get a smaller minimum difference value at $\approx 10^{-5}$, but we reach it at lower depths, and therefore lower numbers of parameters. The accuracy furthermore increases more with depth, even at already high depths. The combined ansatz therefore seems to need a much lower number of parameters to get to the same accuracy as the general ansatz, but the accuracy is limited at a threshold which is lower than the maximum possible accuracy we can reach with the general ansatz at much higher depths. However, this could also be due to convergence behaviour of the optimizer, so this implication is only speculative.

Depth	Combined ansatz	General ansatz
1	29	30
2	47	60
3	65	90
4	83	120
5	101	150
6	119	180
7	137	210
8	155	240

Table 3: Number of parameters depending on depth of the combined ansatz and the general ansatz for a chain length of 4.

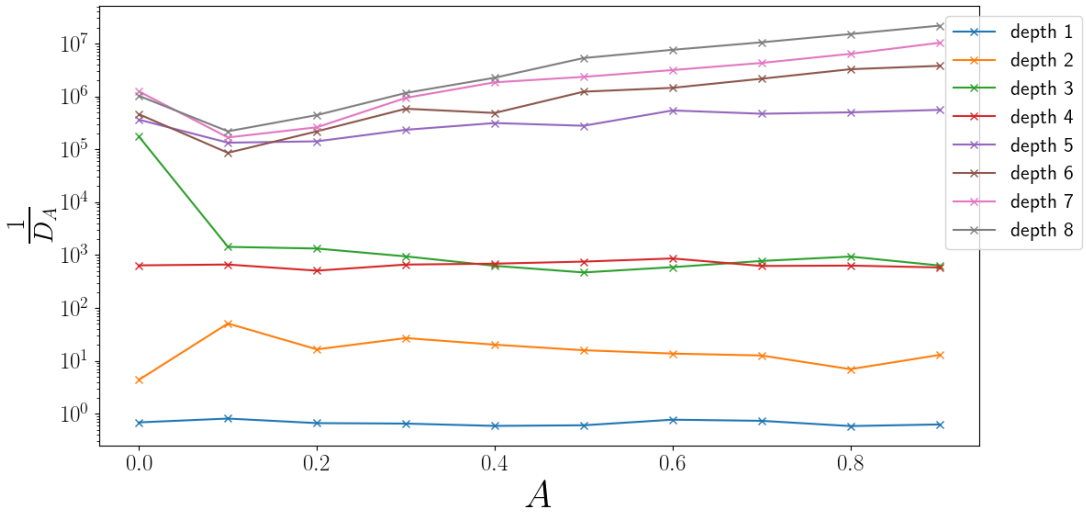

(a) General ansatz

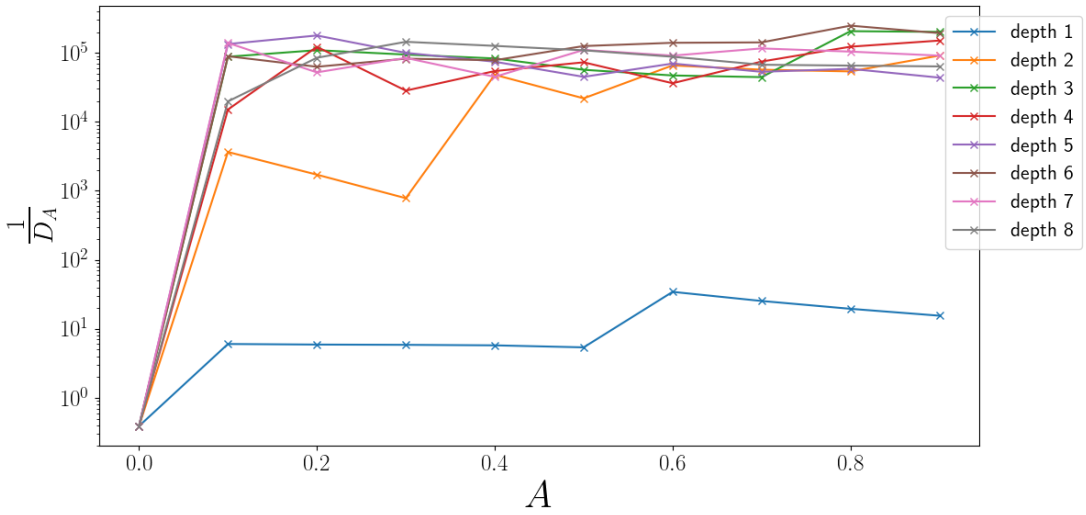

(b) Combined ansatz

Figure 10: Comparison of the combined ansatz and the general ansatz for a chain length of 4 and an initial external field amplitude $A = 0$ with a stepwise increase of 0.1. We can basically make the same observations as for the case of chain length 3, except that the general ansatz, as expected, needs a higher depth to give a good approximation of the eigenstates, which does not seem to be the case for the combined ansatz. What we can see very well in this plot is that the accuracy of the general ansatz, as opposed to the combined one, seems to increase still with higher depths, even beyond depth 6.

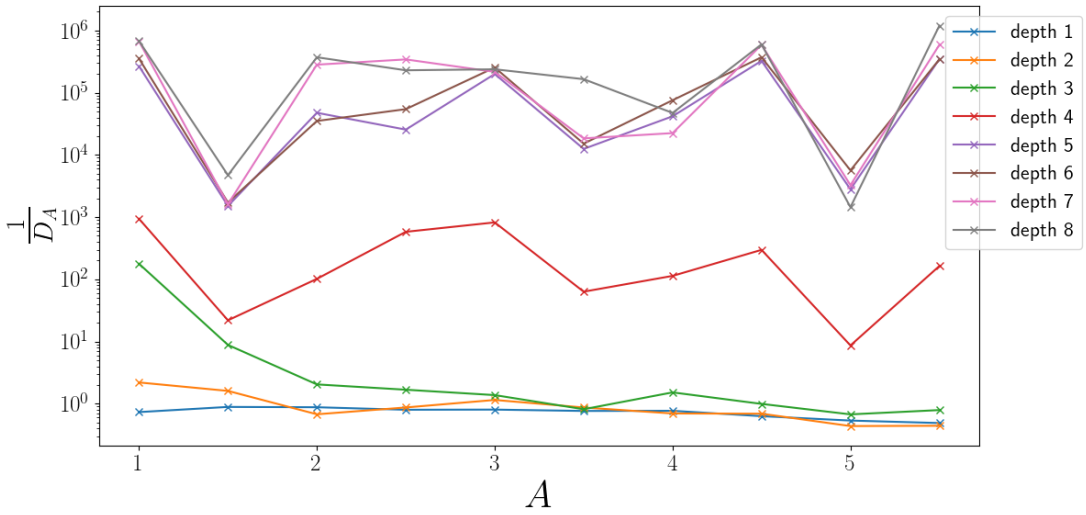

(a) General ansatz

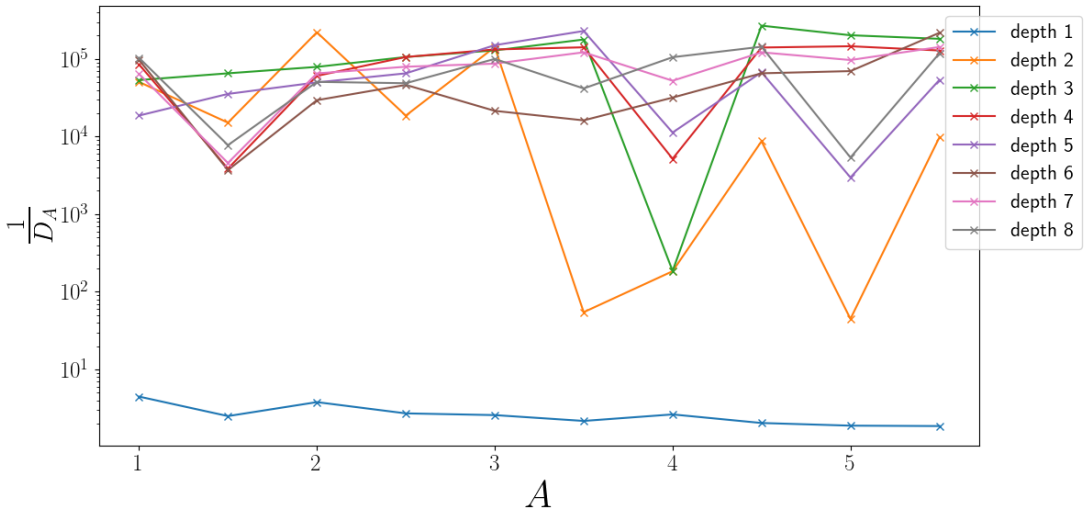

(b) Combined ansatz

Figure 11: Comparison of the combined ansatz and the general ansatz for a chain length of 4 and an initial external field amplitude $A = 1$ with a stepwise increase of 0.5. The observations are again similar to the ones made for chain length 3. Here we can also see well that the combined ansatz of depth 2 seems to have performed a little worse than the ones of higher depths, hinting also a depth scaling of this ansatz, albeit much lower than the one in case of the general ansatz.

Chain length 5

For a chain length of 5 we could not obtain a full set of data points like for the other chain lengths, since especially in the case of the general ansatz with lower depths the program runtime was very high. The fact that the program could not even find the eigenvalues for the starting value of A in this time, however, is a strong indicator for the fact that for these depths, the general ansatz does not perform well. The comparison is shown in figure 12. This would suggest that the general ansatz has acceptable accuracy only for a depth 7 or higher. In case of the combined ansatz, again even for a depth of 2 we already seem to get a good approximation for the eigenstates. Therefore, the depth scaling for the combined ansatz again seems to be a lot lower that the one for the general ansatz. This again means a much higher number of needed parameters in case of the general ansatz, seen in table 4. These findings, however, would require further confirmation, since the data is incomplete.

Depth	Combined ansatz	General ansatz
1	53	38
2	88	76
3	123	114
4	158	152
5	193	190
6	228	228
7	263	266
8	298	304

Table 4: Number of parameters depending on depth of the combined ansatz and the general ansatz for a chain length of 5.

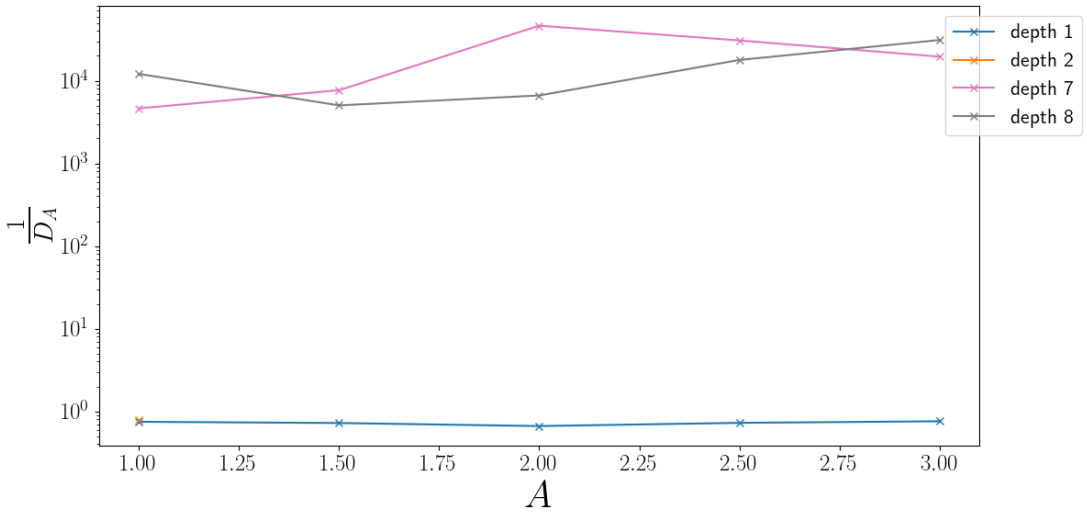

(a) General ansatz

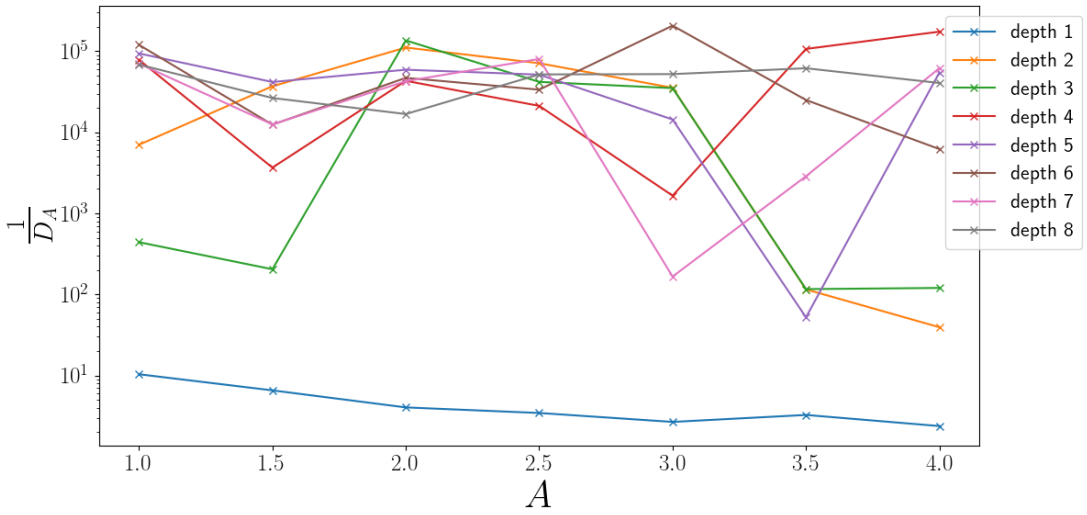

(b) Combined ansatz

Figure 12: Comparison of the combined ansatz and the general ansatz for a chain length of 5 and an initial external field amplitude $A = 0$ with a stepwise increase of 0.1. Here, we do not have as many datapoints due to the high runtime of the algorithm. This was a big problem in particular for the general ansatz with depths 2 to 6. However, the slow convergence of the optimizer in those cases suggests that the ansatz could not reach the eigenstates well. The combined ansatz again seems to perform reasonably well even at depths 2 and 3, wich again suggests a much lower depth scaling as for the general ansatz, but since we do not have much data, we can not make a definite statement about this.

5 Conclusion

In this work, we have presented the Fauseweh-Zhu-2 algorithm to treat Floquet dynamics using a variational quantum algorithm. We developed an ansatz construction scheme for a mixed qubit-qudit architecture, which we implemented and evaluated for this algorithm. In section 2 we first introduced the basics of Floquet formalism, including the method of Floquet matrix as a numerical method to treat Floquet dynamics. We then introduced variational quantum algorithms and presented the Fauseweh-Zhu-2 algorithm as a way to treat Floquet dynamics using this numerical method as introduced in [6]. We furthermore introduced a diagrammatic way to construct an ansatz for a variational quantum algorithm taken from [22]. In section 3 we then constructed the implementation of the Fauseweh-Zhu-2 algorithm we evaluated in this work. We developed an extension for the algorithm to address an issue with degenerate eigenvalues. Furthermore, we presented another, more naive ansatz construction method which is less efficient but more general than the diagrammatic one. We then combined both the naive and the diagrammatic method to develop a problem-specific ansatz construction scheme for a mixed qubit-qudit architecture. We used this scheme to construct an ansatz for the algorithm and implemented the algorithm with this combined ansatz and a general, not problem-specific ansatz for comparison. The algorithm was evaluated for spin-chains of various lengths, driven by an external field. The numerical results are presented in section 4. First, we confirmed the relevance of the extension of the algorithm, showing a high increase in accuracy a high amplitude of the external field. For the general ansatz, we see a dependency on the depth, where the accuracy increases with depth. This corresponds to the results seen also in [25]. For the combined ansatz, we can see the same tendency, however, for the tested examples, the combined ansatz performed better than the general one at much lower depths, implying a much lower depth scaling for the combined ansatz. These first results suggest a strong improvement over a general ansatz at lower depths, so that the combined ansatz needs a much lower number of parameters to reach the same accuracy as the general ansatz. However, we only considered relatively small system sizes, so it would need further work to confirm these findings for more complex systems. For higher depths the general ansatz seems to be able to reach a better maximum accuracy than the combined ansatz, although the confirmation of this, too, would require further work.

Due to long runtimes for higher system sizes, the systems considered in this work are relatively simple examples. This leaves the study of this approach for higher system sizes and higher truncation values $j_{\max}$ as a possibility for further work. Furthermore, we were unable to fully explain some of the data collected in the work, namely the extreme inaccuracy of the combined ansatz for $A = 0$ and the difference in depth scalings at high depths between the general and the combined ansatz. Another important aspect not covered in this work is the effect of qubit noise on the performance of the algorithm and the ansatz. Since all the implementation in this work was done on a classical computer, studying the algorithm on real quantum hardware would be necessary to properly evaluate

its performance.

References

[1] Y. H. Wang, H. Steinberg, P. Jarillo-Herrero, and N. Gedik, "Observation of floquet-bloch states on the surface of a topological insulator," *Science*, vol. 342, no. 6157, pp. 453–457, 2013. [Online]. Available: https://www.science.org/doi/abs/10.1126/science.1239834

[2] H. Miyake, G. A. Siviloglou, C. J. Kennedy, W. C. Burton, and W. Ketterle, "Realizing the harper hamiltonian with laser-assisted tunneling in optical lattices," *Phys. Rev. Lett.*, vol. 111, p. 185302, Oct 2013. [Online]. Available: https://link.aps.org/doi/10.1103/PhysRevLett.111.185302

[3] X. Xi, B. Yan, and L. Yang et al., "Topological antichiral surface states in a magnetic weyl photonic crystal," *Nat Commun*, vol. 14, 2023. [Online]. Available: https://doi.org/10.1038/s41467-023-37710-7

[4] A. Cavalleri, "Photo-induced superconductivity," *Contemporary Physics*, vol. 59, no. 1, pp. 31–46, 2018. [Online]. Available: https://doi.org/10.1080/00107514.2017.1406623

[5] P. Hänggi, "Driven quantum systems."

[6] B. Fauseweh and J.-X. Zhu, "Quantum computing Floquet energy spectra," *Quantum*, vol. 7, p. 1063, Jul. 2023. [Online]. Available: https://doi.org/10.22331/q-2023-07-20-1063

[7] M. Demmer, R. Fonseca, and F. Koushanfar, "Richard feynman: Simulating physics with computers," jan 2008.

[8] M. Nielsen and I. Chuang, *Quantum Computing and Quantum Information*. Cambridge University Press, 2000.

[9] J. Preskill, "Quantum computing in the NISQ era and beyond," *Quantum*, vol. 2, p. 79, aug 2018. [Online]. Available: https://doi.org/10.22331%2Fq-2018-08-06-79

[10] M. Cerezo, A. Arrasmith, and R. Babbush et al., "Variational quantum algorithms," *Nat Rev Phys 3*, sep 2021.

[11] G. Floquet, "Sur les équations différentielles linéaires à coefficients périodiques," *Ann. de l'École Norm. Sup.*, vol. 12, no. 47, 1883.

[12] N. Tsuji, T. Oka, and H. Aoki, "Correlated electron systems periodically driven out of equilibrium: Floquet + DMFT formalism," *Phys. Rev. B*, vol. 78, p. 235124, Dec 2008. [Online]. Available: https://link.aps.org/doi/10.1103/PhysRevB.78.235124

[13] F. Heidrich-Meisner, I. González, K. A. Al-Hassanieh, A. E. Feiguin, M. J. Rozenberg, and E. Dagotto, "Nonequilibrium electronic transport in a one-dimensional mott insulator," *Phys. Rev. B*, vol. 82, p. 205110, Nov 2010. [Online]. Available: https://link.aps.org/doi/10.1103/PhysRevB.82.205110

[14] K. I. Seetharam, C.-E. Bardyn, N. H. Lindner, M. S. Rudner, and G. Refael, "Controlled population of floquet-bloch states via coupling to bose and fermi baths," *Phys. Rev. X*, vol. 5, p. 041050, Dec 2015. [Online]. Available: https://link.aps.org/doi/10.1103/PhysRevX.5.041050

[15] L. D'Alessio, Y. Kafri, A. Polkovnikov, and M. Rigol, "From quantum chaos and eigenstate thermalization to statistical mechanics and thermodynamics," *Advances in Physics*, vol. 65, pp. 239–362, 2016.

[16] M. Moskalets and M. Büttiker, "Floquet scattering theory of quantum pumps," *Phys. Rev. B*, vol. 66, p. 205320, Nov 2002. [Online]. Available: https://link.aps.org/doi/10.1103/PhysRevB.66.205320

[17] T. S. Cubitt, "Dissipative ground state preparation and the dissipative quantum eigensolver," 2023.

[18] Y. Du, M.-H. Hsieh, T. Liu, and D. Tao, "Expressive power of parametrized quantum circuits," *Phys. Rev. Res.*, vol. 2, p. 033125, Jul 2020. [Online]. Available: https://link.aps.org/doi/10.1103/PhysRevResearch.2.033125

[19] J. R. McClean, J. Romero, R. Babbush, and A. Aspuru-Guzik, "The theory of variational hybrid quantum-classical algorithms," *New Journal of Physics*, vol. 18, no. 2, p. 023023, feb 2016. [Online]. Available: https://dx.doi.org/10.1088/1367-2630/18/2/023023

[20] A. Kandala, A. Mezzacapo, and K. Temme et al., "Hardware-efficient variational quantum eigensolver for small molecules and quantum magnets," *Nature*, vol. 549, 242-246, 2017. [Online]. Available: https://www.nature.com/articles/nature23879

[21] W. Fulton, "Eigenvalues, invariant factors, highest weights, and schubert calculus," 2000.

[22] Y. Herasymenko and T. E. O'Brien, "A diagrammatic approach to variational quantum ansatz construction," nov 2021.

[23] R. Fletcher, "Practical methods of optimization," 1988. [Online]. Available: https://api.semanticscholar.org/CorpusID:123487779

[24] "Gsl - gnu scientific library." [Online]. Available: https://www.gnu.org/software/gsl/

[25] C. Bravo-Prieto, J. Lumbreras-Zarapico, L. Tagliacozzo, and J. I. Latorre, "Scaling of variational quantum circuit depth for condensed matter systems," 2020.